Hadronic observables from SIS to SPS energies – anything strange with strangeness ?

H. Weber[1], E. L. Bratkovskaya[1*], W. Cassing[2] and H. Stöcker[1,3]

[1] Institut für Theoretische Physik, Universität Frankfurt

60054 Frankfurt, Germany

[2] Institut für Theoretische Physik, Universität Giessen

35392 Giessen, Germany

[3] SUBATECH, Laboratoire de Physique Sabatomique et des Technologies Associées

University of Nantes - IN2P3/CNRS - Ecole des Mines de Nantes

4 rue Alfred Kastler, F-44072 Nantes, Cedex 03, France

Abstract

We calculate $p, \pi^\pm, K^\pm$ and $\Lambda(+\Sigma^0)$ rapidity distributions and compare to experimental data from SIS to SPS energies within the UrQMD and HSD transport approaches that are both based on string, quark, diquark $(q, \bar{q}, qq, \bar{q}\bar{q})$ and hadronic degrees of freedom. The two transport models do not include any explicit phase transition to a quark-gluon plasma (QGP). It is found that both approaches agree rather well with each other and with the experimental rapidity distributions for protons, Λ's, $\pi^\pm$ and $K^\pm$. In-spite of this apparent agreement both transport models fail to reproduce the maximum in the excitation function for the ratio K^+/π^+ found experimentally between 11 and 40 A·GeV. A comparison to the various experimental data shows that this 'failure' is dominantly due to an insufficient descrip-

arXiv:nucl-th/0209079 v2   6 Dec 2002

tion of pion rapidity distributions rather than missing 'strangeness'. The modest differences in the transport model results – on the other hand – can be attributed to different implementations of string formation and fragmentation, that are not sufficiently controlled by experimental data for the 'elementary' reactions in vacuum.

I. INTRODUCTION

The ultimate goal of relativistic nucleus-nucleus collisions is to reanalyse the early 'big-bang' under laboratory conditions and to find the 'smoking gun' for a phase transition from the expected initial quark-gluon plasma (QGP) to a phase characterized by an interacting hadron gas [1–3]. Though evidence for a 'new phase of hadronic matter' at the SPS has been claimed [4], a direct proof – according to the understanding of the authors – is still lacking [5,6]. Furthermore, nucleus-nucleus collisions with initial energies per nucleon of ≈ 21.3 A·TeV ($\sqrt{s} = 200$ GeV) are available now at the Relativistic-Heavy-Ion-Collider (RHIC) in Brookhaven, an order of magnitude higher than at SPS energies ($\sqrt{s} \approx 17$-19 GeV). In central collisions of Au + Au nuclei here energy densities above 4 GeV/fm^3 are expected [6]. These estimates are based on the Bjorken prescription [7] employing a formation time of $\tau = 1$ fm/c. The latter quantity is uncertain by at least a factor of 2 which implies a corresponding uncertainty in the energy density. Nevertheless, energy densities of a few GeV/fm^3 suggest that the critical energy density for a QGP phase should be overcome in considerable space-time volumes at RHIC, where the relevant degrees of freedom are partons (quarks and gluons). Parton cascade calculations [8–10] are expected to provide suitable descriptions in the early phase [11,12] of these collisions whereas hadrons should only be formed (by 'condensation') at a later stage which might be a couple of fm/c from the initial contact of the heavy ions. In fact, hybrid models like VNI+UrQMD [13], VNI+HSD [14] or the AMPT approach [15] also allow for a reasonable description of the 'soft' hadronic observables so far, which – due to the high interaction rate – are found to be close to the hydrodynamic limit [16]. On the other hand, once the local equilibrium limit is reached in the reaction, any conclusion on the dynamics in the early nonequilibrium phase and its dynamical degrees of freedom becomes highly model dependent.

Moreover, the question of chiral symmetry restoration at high baryon density and/or high temperature is of fundamental interest, too [1,2]. Whereas lattice QCD calculations at zero baryon chemical potential indicate that a restoration of chiral symmetry goes along

with the deconfinement phase transition at a critical temperature T_c, the situation is less clear at finite baryon density where QCD sum rule studies show a linear decrease of the scalar quark condensate $\langle \bar{q}q \rangle$ – which is nonvanishing in the vacuum due to a spontaneous breaking of chiral symmetry – with baryon density ρ_B towards a chiral symmetric phase characterized by $\langle \bar{q}q \rangle = 0$. This decrease of the scalar condensate is expected to lead to a change of the hadron properties with density and temperature, i.e. in a chirally restored phase the hadrons might become approximately massless as suggested in Ref. [17]. However, chiral symmetry restoration only implies that vector and axial vector currents should become equal [18,19]. Thus vector and axial vector excitations of the QCD vacuum must have the same spectral functions in the chiral limit. As demonstrated in Refs. [20,21] such a restoration of chiral symmetry in central nucleus-nucleus collisions should — driven by the baryon density — occur at bombarding energies of 5–10 A·GeV. In Ref. [22] it has been argued, furthermore, that such 'phase transitions' should be seen in a much lower strangeness to entropy ratio. It has been also suggested [21] that especially the K^+/π^+ might give an indication for a chirally restored phase.

The fact that the K^+/π^+ ratio is found experimentally to be higher at top AGS energies of 11 A·GeV than at 160 A·GeV has raised speculations about the appearance of 'new physics' at energies between AGS and top SPS. To shed some light on this issue, the NA49 Collaboration has started an energy scan at the SPS. First results have become available now at 40 and 80 A·GeV [23–25] and further studies are foreseen at 30 and 20 A·GeV [26]. Since this topic is of current interest we will restrict our investigations to the AGS and SPS energy range in this paper.

From the theoretical side the various hadron spectra are conventionally calculated with nonequilibrium kinetic transport theory (cf. [27–32]). However, the calculated kaon to pion ratio from central nucleus-nucleus collisions turns out to vary by factors as large as 2 if different transport approaches are applied [21,33,34,32]. Thus a unique interpretation of the data is questionable so far. On the other hand, statistical models [35] show a maximum of K^+/π^+ ratio at ~ 30 A·GeV since the relative strangeness content of baryons is highest at low bombarding energies. It decreases with higher energies due to an increase

4

of temperature and a decrease of the baryon chemical potential. However, an analysis within the UrQMD transport model suggests that chemical and thermal equilibria are achieved only briefly in a small central overlap region of heavy-ion collision due to a very fast expansion of the hadronic fireball [36]. Moreover, the analysis of Ref. [37] within the HSD transport approach indicates that the equilibration time for strangeness at all bombarding energies is larger ($\geq$ 40 fm/c) than the reaction time of nucleus-nucleus collisions. Thus the statistical model fits to the data have to be considered with some caution since they are not understood microscopically.

In this work we concentrate on hadronic rapidity distributions of protons, kaons, antikaons and hyperons and their yields and ratios from $Au + Au$ (or $Pb + Pb$) collisions from SIS to SPS energies. The aim of our study is twofold: first, to find out the systematic differences between two currently used transport approaches (denotes as UrQMD [38,39] and HSD [27,40]) and second, to look for common failures in comparison to related experimental data that have become available recently [23–25] or provide predictions for experimental studies in the near future [26], which are also of relevance for the new GSI-proposal [41].

Our work is organized as follows: In Section 2 we will describe the main ingredients of the UrQMD and HSD transport approaches and point out conceptual differences. In Section 3 we study baryon stopping in central $Au + Au$ collisions from 4 to 160 A·GeV in comparison to experimental data (whenever available). Section 4 is devoted to a detailed comparison of both transport approaches on $\pi^{\pm}, K^{+}, K^{-}$ and $\Lambda+\Sigma^0$ rapidity distributions, yields and different particle ratios as a function of bombarding energy from 2 to 160 A·GeV. Again the calculations will be confronted with experimental data taken at the AGS and SPS. A direct comparison of UrQMD and HSD on the pp and $\pi^- p$ reaction level is given in Section 5 to quantify the differences in the 'elementary' differential cross sections. Section 6 concludes our study with a summary and discussion of open problems.

II. TRANSPORT MODELS – URQMD AND HSD

In this work we employ two different transport models, i.e. the UrQMD and HSD approaches, that have been used to described nucleus-nucleus collisions from SIS to SPS energies for several years. Though different in the numerical realisation, both models are based on the same concepts: string, quark, diquark ($q, \bar{q}, qq, \bar{q}\bar{q}$) and hadronic degrees of freedom. It is important to stress that both approaches do not include any explicit phase transition to a quark-gluon plasma (QGP). The philosophy is that a common failure of both models in comparison to experimental data should – model independently – indicate the appearance of 'new physics'.

The UrQMD (Ultra-relativistic Quantum Molecular Dynamics) transport approach is described in Refs. [38,39]. It includes all baryonic resonances up to an invariant mass of 2 GeV as well as mesonic resonances up to 1.9 GeV as tabulated in the PDG [42]. For hadronic continuum excitations a string model (let's denote it as 'Frankfurt' string model (FSM)) is used. The hadron formation time (which relates to the time between the formation and fragmentation of the string in the individual hadron-hadron center-of-mass frame) is in the order of 1-2 fm/c depending on the momentum and energy of the created hadrons (using the "yo-yo" formation concept for the time definition) [38,39]. The UrQMD transport approach is matched to reproduce nucleon-nucleon, meson-nucleon and meson-meson cross section data in a wide kinematical regime [38,39]. At the high energies considered here the particles are essentially produced in primary high energy collisions by string excitation and decay, however, the secondary interactions among produced particles (e.g. pions, nucleons and excited baryonic and mesonic resonances) – that also contribute to the particle dynamics – are included as well.

Whereas UrQMD operates as default in the cascade mode, i.e. with hadron potentials turned off, the HSD (Hadron-String Dynamics) transport approach includes (by default) scalar and vector fields of the particles which determine the mean-field propagation of the hadrons between collisions (cf. Fig. 2 of Ref. [21]). The HSD transport approach incorporates only the baryon octet and decuplet states and N*(1440), N*(1535) as well

as their antiparticles and the 0^- and 1^- meson octets. Higher baryonic resonances are discarded as explicit states (for propagation) in HSD; they are supposed to "melt" in the nuclear medium even at normal nuclear density (see e.g. [43,44]). The argument here is that the resonance structure (above the Δ-peak) is not seen experimentally even in photoabsorption on light nuclei [45]. In contrast to the resonance concept – adopted in UrQMD for all low energy baryon-baryon and meson-baryon collisions – HSD includes the direct (non-resonant) meson production in order to describe the corresponding cross sections (for the details see Ref. [27]).

In the HSD approach the high energy inelastic hadron-hadron collisions are described by the LUND string model (realized by FRITIOF-7.02 [46]), where two incoming hadrons emerge from the reaction as two excited color singlet states, i.e. 'strings' (as in UrQMD). The formation time of all hadrons — composed of light and strange quarks — in HSD is assumed to be $\tau_F \sim 0.8$ fm/c in the hadron rest frame [27,40], which is lower than the 'average' of the exponentially distributed formation times of 1–2 fm/c used in UrQMD. Note, that in both models the formation time in the calculational frame for heavy-ion collisions (laboratory or center-of-mass frame) is dilated by the Lorentz γ-factor, i.e. $t_F = \gamma \cdot \tau_F$.

Since at high energy heavy-ion collisions particle production essentially proceeds via baryon-baryon and meson-baryon string excitations and decays, it is worth to discuss the differences in the realizations of the string models used in UrQMD and HSD. In both string models the production probability P of massive $s\bar{s}$ or $qq\bar{q}\bar{q}$ pairs is suppressed in comparison to light flavor production ($u\bar{u}$, $d\bar{d}$) according to a generalized Schwinger formula [47]

$$\frac{P(s\bar{s})}{P(u\bar{u})} = \frac{P(s\bar{s})}{P(d\bar{d})} = \gamma_s = \exp\left(-\pi\frac{m_s^2 - m_q^2}{2\kappa},\right) \tag{1}$$

with the string tension $\kappa \approx 1$ GeV/fm. Thus in the string picture the production of strangeness and baryon-antibaryon pairs is controlled by the masses of the constituent quarks and diquarks. Inserting the constituent quark masses $m_u = 0.3$ GeV and $m_s = 0.5$ GeV a value for the strangeness suppression factor $\gamma_s \approx 0.3$ is obtained. While

the strangeness production in proton-proton collisions at SPS energies is reasonably well reproduced in the LUND string model with $\gamma_s = 0.3$, the strangeness yield for $p + Be$ collisions at AGS energies (which is a good probe for the isospin averaged elementary $p+p$ and $p + n$ reactions) is underestimated by roughly 30% [33]. Therefore the strangeness suppression factor has been enhanced to 0.4 at AGS energies for the elementary nucleon-nucleon cross section in HSD. Thus, the relative production probabilities for the different quark flavours in the HSD model are

$$\text{HSD}: \quad u : d : s : diquark = \begin{cases} 1 : 1 : 0.3 : 0.07 \text{ for } \sqrt{s} \geq 20 \text{ GeV} \\ 1 : 1 : 0.4 : 0.07 \text{ for } \sqrt{s} \leq 5 \text{ GeV} \end{cases} \tag{2}$$

with a linear transition of the strangeness suppression factor as a function of $\sqrt{s}$ in between. The relative production probabilities for the different quark flavors in UrQMD are fitted to

$$\text{UrQMD}: \quad u : d : s : diquark = 1 : 1 : 0.35 : 0.1. \tag{3}$$

Additionally fragmentation functions $f(x, m_t)$ must be specified, which are the probability distributions for hadrons with transverse mass m_t to acquire the energy-momentum fraction x of the fragmenting string. One of the most common fragmentation functions is used in the LUND model [46] (which is adopted in the HSD approach [33])

$$f(x, m_t) \approx \frac{1}{x}(1 - x)^a \exp\left(-bm_t^2/x\right), \tag{4}$$

with $a = 0.23$ and $b = 0.34$ GeV^{-2}. In UrQMD different fragmentation functions are used for leading nucleons and newly produced particles, respectively (cf. Ref. [38] Fig. 3.16):

$$f(x)_{\text{nucl}} = \exp\left(-\frac{(x - B)^2}{2A}\right), \text{ for leading nucleons}$$
$$f(x)_{\text{prod}} = (1 - x)^2, \text{ for produced particles} \tag{5}$$

with $A = 0.275$ and $B = 0.42$. The fragmentation function $f(x)_{\text{prod}}$ — used for newly produced particles — is the well-known Field-Feynman fragmentation function [48]. At the string break-up the $q\bar{q}$-pairs have zero transverse momenta in the string reference frame,

but the transverse momentum distributions of the single quark $(\vec{p}_t)$ and the corresponding antiquark $(-\vec{p}_t)$ are taken to be gaussian

$$f(p_t) = \frac{1}{\sqrt{\pi\sigma^2}} \exp\left(-\frac{p_t^2}{\sigma^2}\right) \tag{6}$$

with $\sigma = 1.6$ GeV/c.

Despite the differences in the fragmentation functions, both string models describe quite well the data available for particle multiplicities and total spectra from pp collisions at high energies (see Ref. [38] for UrQMD and Ref. [33] for HSD). Also the inelastic pion-proton cross section is in good agreement with the experimental data in both models whereas differential spectra can differ substantially (cf. Section V). The LUND string model (in HSD) has also been tested for low energy pp collisions as well as for πN interactions (cf. Chapter 2 in Ref. [33]). It has been shown that the (LUND) string model underestimates pion and kaon/antikaon yields closer to their production threshold. In HSD the threshold for string formation and decay thus is taken as $\sqrt{s} = 2.6$ GeV for baryon-baryon collisions and at $\sqrt{s} = 2.1$ GeV for meson-baryon collisions. For lower invariant energies $\sqrt{s}$ resonant and direct meson production mechanisms (e.g. $\pi N \to N\pi\pi$) dominate, which are implemented in addition in HSD to ensure smooth excitation functions of the meson multiplicities from threshold to a few hundred GeV/c.

III. BARYON STOPPING

Though various predictions have been made in both transport models since a couple of years, it is of importance to compare with actual data. We employ the experimental cuts in centrality to get as realistic as possible in the comparison of baryon stopping achieved in both theoretical approaches and in the different experiments. A related comparison is presented in Fig. 1 for protons from 5% (4, 6, 8, 10.7 and 160 A·GeV) and 7% central (20, 40, 80 A·GeV) $Au + Au$ (AGS) and $Pb + Pb$ (SPS) collisions at 4–160 A·GeV [1].

---

[1]Note, that for all UrQMD and HSD calculations presented in this work the centrality of the reaction has been determined by a comparison of the transport calculations to the energy

The experimental data at 4, 6, 8, 10.7 A·GeV have been taken from Ref. [49] (circles), at 160 A·GeV from [50] (triangles) and from [51] (circles). The full symbols (here and for all further figures) correspond to the measured data whereas the open symbols are the data reflected at midrapidity. The solid lines with stars show the results from the UrQMD calculations while the solid and dashed lines stem from the HSD approach with and without potentials, respectively.

We note, that in the UrQMD calculations 'spectator' protons have been cut off whereas they are still present in the HSD calculations; this leads to the maxima in the proton rapidity distributions at target and projectile rapidity in the HSD calculations (cf. Fig. 1). Nevertheless, the HSD cascade calculations are found to agree with UrQMD cascade calculations from 4–20 A·GeV within 5%, whereas UrQMD shows somewhat more proton stopping than HSD at higher bombarding energies. The mean-field propagation effects in the HSD approach are most pronounced at low bombarding energies leading to a reduction of baryon stopping from 4 – 10.7 A·GeV and a flatter rapidity distribution dN/dy around midrapidity slightly closer to the experimental data. This effect can easily be attributed to the energy stored in the repulsive mean field at high baryon density and moderate bombarding energy. Above about 40 A·GeV such potential effects are no longer statistically significant in the calculations since the repulsive mean field decreases strongly with momentum (cf. Fig. 2 of Ref. [21]) such that at 40 A·GeV no repulsion is seen by the nucleons in the initial high density phase. Only when the system partly thermalizes and the nucleon momenta relative to the fireball reference frame become smaller the baryons 'feel' again a repulsive mean field, however, now at rather low baryon density. We recall that at density ρ_0 the potential is even attractive for momenta ≤ 600 MeV/c.

In general the HSD results indicate slightly less baryon stopping than the UrQMD calculations. At 160 A·GeV the experimental data favor a minimum of the distribution

---

distribution in the Veto-calorimeter of the NA49 collaboration for SPS energies and to the New Multiplicity Array (NMA) and ZCAL-calorimeters at AGS energies

at midrapidity, which is reproduced by the HSD calculations. However, the UrQMD calculations only deviate by $\sim 5\%$. We note, that for semi-central and peripheral $Pb+Pb$ collisions at 160 A·GeV the UrQMD calculations are in good agreement with the data from Ref. [50] (cf. Fig. 1 in Ref. [52]).

Thus, the overall description of the rapidity spectra from both models (with/without potentials) in this wide energy regime is quite remarkable in view of the different 'hadronic' degrees of freedom and string 'parameters' involved.

IV. PION AND STRANGENESS PRODUCTION

We continue with $\pi^{\pm}, K^{+}, K^{-}$ and $\Lambda + \Sigma^0$ rapidity spectra in 5%, 7%, or 10% central collisions of $Au+Au$ or $Pb+Pb$, respectively, from 4–160 A·GeV. We compare to the AGS data from Refs. [53–58] in Fig. 2 and SPS data from Refs. [23–25] in Fig. 3. Here the thick solid lines denote the HSD results including the potentials, the dashed lines represent HSD calculations in the cascade mode, which should be directly compared to the UrQMD results (thin solid lines with stars). Both Figs. – taken together – provide an overview on the energy dependence of the different rapidity distributions and the virtues/failures of the transport models.

At 4 A·GeV all transport versions overestimate the π^+ spectra. This deviation is most pronounced in the HSD 'cascade' version. On the other hand, UrQMD is higher than HSD in the strangeness channels $K^{\pm}$ and $\Lambda + \Sigma^0$, whereas HSD (with potentials) is quite compatible with the midrapidity data. At 6 A·GeV the HSD (with potential) calculations are in line with the experimental $K^{\pm}$ and $\Lambda + \Sigma^0$ data whereas the UrQMD results are still too high. All calculations again overestimate the π^+ rapidity spectra. At 8 A·GeV the UrQMD and HSD results continue to overestimate the π^+ yield, while now the HSD calculations (with potential) fall low in the strangeness channels contrary to the HSD cascade and UrQMD results. At 10.7 A·GeV the picture continues: both models give too many π^+, the strangeness yield is approximately reproduced in the cascade versions and underestimated in the HSD simulation with potentials.

At 20 A·GeV, most relevant for the future GSI facility [41], both transport models (with/without potentials) give the same rapidity distributions for all hadrons considered here. Note, that the cascade HSD results are not shown explicitly in Fig. 3 since the cascade and potential results are practically coincident. As discussed above this is due to the momentum-dependence of the scalar and vector potentials in HSD; both potentials vanish for relative momenta of a couple of GeV/c. Deviations between HSD and UrQMD come up again at 40 A·GeV, where UrQMD now gives more π^- and lacks a few K^+, whereas the K^- and $\Lambda + \Sigma^0$ spectra are reasonably reproduced. At this energy HSD (with/without potentials) only overestimates the π^- distribution slightly. At 80 A·GeV the UrQMD spectra are also fine for K^- and Λ, but low for K^+ and too high for π^-. At 160 A·GeV the HSD calculations indicate slightly too few π^- at midrapidity, however, do well for $K^\pm$ and $\Lambda + \Sigma^0$ as already demonstrated earlier in Refs. [27,33]. The UrQMD results here show too many π^+ and a slightly higher $\Lambda + \Sigma^0$ yield, whereas the K^+ distribution is underestimated. We note, that the UrQMD results presented in Fig. 3 are taken from Ref. [34].

As a more general overview on the $\pi^\pm$ abundancies in central $Au + Au$ and $Pb + Pb$ collisions we show in Fig. 4 the π^+ (upper plots) and π^- (lower plots) multiplicities at midrapidity (left column) and integrated over rapidity (right column) as a function of the bombarding energy in comparison to the available data from Refs. [23,53]. Here the solid lines with open triangles show the results from the UrQMD calculations while the solid lines with open squares and dashed lines stem from the HSD approach with and without potentials, respectively. At lower AGS energies the UrQMD model gives slightly less pions then HSD (with/without potential), but both models overpredict the midrapidity data (except UrQMD at 2 A·GeV, which is in line with data point at midrapidity). About 20 A·GeV is the "crossing point" for both transport calculations and at SPS energies the tendency turns around: UrQMD gives more pions than HSD, so that HSD is now in a better agreement with the experimental data.

The overestimation of the pion yield at low and high energies by the transport models is presently not well understood. In Ref. [59] Larionov et al. have speculated that higher

baryon resonances – more massive than the Δ-resonance – might be quenched at densities above $\sim 1.5 \, \rho_0$ both in NN as well as πN channels. The net effect at SIS energies (and slightly higher bombarding energies) is a reduction of the pion yield in collisions of heavy systems such as $Au+Au$ whereas light systems (e.g. $C+C$) are not effected very much [59]. Though this might be a possible explanation at SIS and lower AGS energies, other effects such as strong pion self energies could also lead to a reduction of the pion abundance in the transport models. Such many-body effects have not been incorporated in the calculations presented here. At SPS energies and especially at 160 A·GeV another production channel for pions becomes sizeable, i.e. the annihilation of baryon-antibaryon ($B\bar{B}$) pairs that leads on average to 5 pions (or more). However, by employing detailed balance on the many-body level [60] the $B\bar{B}$ annihilation rate is found to be almost compensated by many-meson fusion channels that recreate $B\bar{B}$ pairs. This many-body channel is not incorporated in UrQMD and thus might partly be responsible for the overestimation of the pion yield. A rough estimate, however, shows that this missing channel cannot be the only reason: as calculated in Ref. [60] (and approved by recent NA49 measurements [25]) the $\bar{p}/<\pi>$ ratio ($<\pi> = 0.5(\pi^+ + \pi^-)$) is approximately independent on the centrality of the $Au + Au$ collision and $\sim 1\%$. Assuming the number of $\bar{n}$ to be equal to the number of antiprotons as well as the number of antihyperons [25] and adopting isospin symmetry for the pions, we get $\bar{N}/\pi \approx 1$ %. If all $\bar{N}$'s produced initially are annihilated, which is an upper estimate for the pion production from this channel, then we could achieve a maximum increase of the pion number by 5 %. Thus a $\sim$20 % overestimation of the pion yield by UrQMD at 160 A·GeV can only partly be attributed to the missing multi-meson fusion channels.

The K^+ (upper plots) and K^- (lower plots) multiplicities at midrapidity (left column) and integrated over rapidity (right column) are shown in Fig. 5 as a function of the bombarding energy in comparison to the available data from Refs. [23,53]. Here the midrapidity and total yields summarize the findings from Figs. 2-3: The K^- abundancies are well described by both transport models. The K^+ yield at midrapidity (left column) is slightly overestimated by UrQMD at AGS energies and underestimated at SPS energies,

whereas HSD is in a reasonable agreement with the data except of the upper AGS energies (with potentials included). This tendency stays the same for the 4π kaon yield, however, at SPS energies the difference between both models for the 4π yields is smaller than at midrapidity since UrQMD provides a slightly broader kaon rapidity distribution than HSD (cf. Fig. 3). Thus, an underestimation of strangeness production is not the prevailing issue as demonstrated in Fig. 5 in comparison to the recent experimental data from NA49 [23]. Both transport models can roughly describe - within their systematic range of uncertainties - the $K^{\pm}$ spectra and abundancies.

In Fig. 6 we show the K^+/π^+ and K^-/π^- ratios at midrapidity (left column) and integrated over all angles (right column) as a function of the bombarding energy for central collisions of $Au + Au$ (AGS) or $Pb + Pb$ (SPS) in comparison to the available data from Refs. [23,53]. Whereas the excitation function of the K^-/π^- ratio is roughly reproduced by both transport models, the maximum in the K^+/π^+ ratio seen experimentally both at midrapidity (upper left part) and in 4π (upper right part) is not described by HSD as well as UrQMD. For the K^+/π^+ ratio both models give quite different results. HSD gives a monotonous increase of this ratio with bombarding energy (as pointed out in Refs. [21,33][2]), whereas within UrQMD the ratio shows a maximum around 10 A·GeV and then drops slightly for the midrapidity ratio or stays roughly constant for the 4π ratios. In view of Figs. 2-5 this failure is not primarily due to a mismatch of strangeness production, but more due to an insufficient description of the pion abundancies.

Fig. 7 shows the excitation functions of $\Lambda + \Sigma^0$-hyperons at midrapidity (upper left part) and integrated over all angles (upper right part) as a function of the bombarding energy for central collisions of $Au + Au$ (AGS) or $Pb + Pb$ (SPS) in comparison to the available data from Refs. [24,25,57,58,61]. Here UrQMD (solid lines with open triangles)

---

[2]We note that the HSD results presented in this work are produced with much higher statistics than in Refs. [21,33] due to the increasing computer power available. Also the centrality selection is done now in line with the actual experimental set-up.

slightly underestimates the 4π yields at 40 and 80 A·GeV whereas HSD (solid lines with open squares) seems to give a better description. Nevertheless, all models compare rather well with data.

The $(\Lambda + \Sigma^0)/\pi$ ratios[3] at midrapidity (lower left part) and integrated over 4π (lower right part) are underestimated slightly which should again be attributed to the pion excess in the transport models (see above). Nevertheless, the maxima in the ratios (4π and midrapidity) observed experimentally is qualitatively reproduced by both models indicating that with increasing bombarding energy s-quarks are more frequently produced within mesons ($\bar{K}, \bar{K}^*$) rather than in associate production with baryons. A similar trend is also found in statistical model fits [35].

The excitation function for the K^-/K^+ ratio in central collisions of $Au + Au$ (AGS) or $Pb + Pb$ (SPS) is shown in Fig. 8 for midrapidity ratios (l.h.s.) and in 4π (r.h.s.). Experimental data [23,53] here are only available for the midrapidity ratios. Again we find that both transport models give similar results for this ratio which are comparable to the data. Statistical models also fit this ratio quite well. Whether this finding implies that 'chemical equilibration' is approximately achieved in central collisions of heavy nuclei is still an open question [62].

One note of caution again: the pions in both transport models are treated as 'free' particles, i.e. with their vacuum mass. On the other hand, lattice QCD calculations as well as effective Lagrangian approaches like the Nambu-Jona-Lasinio (NJL) model show that the pion mass should increase with temperature and density. So the overestimation of the pion yields in HSD and UrQMD might be a signature for a dynamically larger pion mass. Moreover, in-medium changes of the strange hadron properties, as known from experimental studies at SIS energies, should also show up at AGS and SPS energies. Thus, including all medium effects simultaneously in a consistent way might provide a more conclusive interpretation of the ratios in Figs. 6-8. However, such calculations require

---

[3]The pion multiplicity is calculated as $\pi = 3/2(\pi^+ + \pi^-)$ in line with Ref. [24,25]

a precise knowledge about the momentum and density dependence of the hadron self-energies which is not available so far. Note, that up to now in-medium modifications of the K^+, K^- properties have been studied with HSD employing a dropping of K^- and increase of K^+ masses in the medium [63]. As summarized in [27] such a scenario leads to an enhancement of K^- and a lowering of K^+ yields at SIS energies (which is close to threshold for K^+, K^- production). It modifies only slightly the strangeness abundancies at SPS energies. However, chiral symmetry restoration also requires a simultaneous modification of the pion properties.

We close this Section with some speculations about the failure of the transport models for the K^+/π^+ ratio at the top AGS energies (and slightly above). To this aim let's assume that the pion yield is decreased by some mechanism to the actual yield observed experimentally. Since kaons and antikaons are also produced in secondary non-strange meson-baryon collisions, this will imply also a reduction of the kaon number in the transport calculations. For central $Au+Au$ reactions these secondary channels give roughly the same amount of kaons and antikaons as the primary NN channels. Thus a 20% decrease in the pion number will lead to a maximum change in the kaon number by 10% and the K^+/π^+ ratio might increase by about 10%, too. This relative increase will improve the situation in comparison to experiment, however, not solve the problem. Another possibility is the enhanced production of $s\bar{s}$ pairs in the hot and dense hadronic medium relative to the vacuum, i.e. an increase of γ_s in Eq. (1). Such modifications might be driven by an enhanced string tension κ in the medium [64] or a relative decrease of $m_s^2 - m_q^2$ with density and temperature. Alternatively, also the formation of a QGP in the initial phase might lead to enhanced strangeness production. According to the authors point of view such phenomena cannot be excluded presently, however, there is also no strong evidence in favor of them.

V. URQMD VERSUS HSD

Though both transport approaches – HSD and UrQMD – give qualitatively and quantitatively similar results for proton, $\pi^{\pm}, K^{\pm}$ and hyperon rapidity distributions, there are quantitative differences that should be cleared up. To this aim we concentrate on idealized model comparisons which are not directly comparable to experimental data.

The excitation functions for s- and $\bar{s}$-quark production in $b = 0$ collisions of $Au + Au$ (AGS) or $Pb + Pb$ (SPS) nuclei (HSD: l.h.s.; UrQMD: r.h.s.) are shown in Fig. 9 which finally end up in mesons or baryons (antibaryons). The solid (dashed) lines with full (open) squares and circles indicate the number of s-quarks ($\bar{s}$-quarks) in baryons (antibaryons) and mesons, respectively. Both models give qualitatively and quantitatively similar results (as already found from the previous comparisons) showing that at ~ 80 A·GeV the same amount of s-quarks end up in mesons and baryons, whereas baryons are preferred at lower energies. The $\bar{s}$-quarks in antibaryons are almost negligible in this energy range. We mention here that strangeness conservation is exactly fulfilled in both transport models such that at all energies the number of s-quarks is identical to the number of $\bar{s}$-quarks.

The channel decomposition (fraction in %) for the finally observed K^{+} (left column) and K^{-} (right column) from HSD (upper part) and UrQMD (lower part) are shown in Fig. 10 as a function of bombarding energy for $Au + Au$ (AGS) or $Pb + Pb$ (SPS) collisions at impact parameter $b = 0$. Note, that only the contributions of the dominant channels are shown in Fig. 10. For a correct interpretation of Fig. 10 one has to keep in mind, that at high energies initially $s, \bar{s}$ quarks are produced in primary nucleon-nucleon collisions and later on in meson-baryon interactions via string excitation and decay. However, subsequently the strange particles (produced initially) participate in chemical reactions with flavor exchanges. As a result only a few percent of the 'primary' kaons/antikaons remain unaffected by secondary inelastic interactions (cf. the lines denoted as 'BB string' in Fig. 10). Most of the final K^{+} and K^{-} mesons – above 10 GeV – finally stem from $K^{*\pm}(892)$ decays (lines '$K^*(892)$ decay') which are either produced directly in string decays or by pion-kaon resonant scattering. As seen from the lower part of Fig. 10,

in UrQMD a large fraction of final K^+, K^- stem directly (without K^* production and decay) from meson-baryon collisions (line 'mB string'). These are realized in UrQMD via an excitation of a single string that furtheron decays isotropically, which is reminiscent of the resonance mechanism. The same mechanism is also used for high energy meson-meson collisions (line 'mm string'). In HSD this channel is treated differently, i.e. via $K^*(892)$ resonance production, and thus contributes to the '$K^*(892)$' channel. Note also, that in UrQMD – in the channel denoted as 'mB string' – the kaon/antikaon-baryon collisions are counted, too, whereas they are not counted here in HSD. In both models only a few percent of the final K^+ and K^- appear from the $\phi(1020)$ meson decays (lines 'ϕ decay'). We mention that only a small fraction of the ϕ-decays can be reconstructed from K^+K^- invariant mass spectra.

The conceptual differences in the treatment of strangeness production in both transport approaches are more pronounced at low energies. UrQMD implements the full resonance dynamics assuming the vacuum resonance properties: At low energies the baryon and meson resonances are excited in baryon-baryon (BB), meson-baryon (mB) or meson-meson (mm) collisions (below the string thresholds) and decay (after time $1/\Gamma$) to K^+, K^- (cf. the line 'N^*' in Fig. 10 denoting the fraction of the final K^+, K^- from strange baryon resonance decays: $N^*(1650)$, $N^*(1710)$, $N^*(1720)$, $N^*(1990)$ and line 'Y^*' for the higher hyperon resonances as well as the lines '$K_1 + K_0^*$' and $a_0 + f_0$ indicating the fraction from the decay of meson resonances: $K_1(1270)$, $K_0^*(1430)$ and $a_0(980)$, $f_0(980)$, respectively). In HSD these high strange baryon and meson resonances are not produced and propagated explicitly (as indicated in Section 2). Instead – in low energy BB, mB or mm collisions – strangeness is directly produced with respect to the corresponding transition rates and 2, 3 or 4-body kinematics for the final states (cf. lines denoted as '$\pi N \rightarrow KY$', '$\pi Y \rightarrow \bar{K}N$' or '$mm$ coll.' in the upper part of Fig. 10). This comparison demonstrates that the individual channels are treated quite differently though the final results are very similar.

Thus, as seen from Fig. 10, only a small fraction of kaons/antikaons (less than 10% of the kaons and less than 6% of the antikaons) from energetic initial baryon-baryon

collisions (cf. lines denoted as BB string) survives the hadronic rescattering phase during the expansion of the fireball without reinteraction. Most of the final strange particles emerge after rescattering — shifting s quarks from mesons to baryons and vice versa — thus providing a very distorted picture of the initial strangeness production mechanism and the elementary degrees of freedom involved. Consequently, as pointed out in Ref. [34], the $K^\pm$ and Λ spectra do not allow for stringent conclusions on the initial phase of high energy density. On the other hand, these frequent flavor exchange reactions may be viewed as the reason why statistical models (employing chemical equilibrium) seem to work reasonably well.

A. pp reactions

In order to get some idea about the differences between both transport approaches we go back to the description of the elementary channels like pp or $\pi^- p$ in vacuum. In this respect we show in Fig. 11 the proton rapidity distributions for pp collisions from HSD (solid lines) and UrQMD (dashed lines) between 4 and 160 GeV laboratory energy. This provides information on the different string excitation and fragmentation schemes. The experimental data at 160 GeV are taken from Ref. [50]. As seen from Fig. 11, however, the differences between the two string fragmentation schemes are only minor. Where do the differences in baryon stopping — shown in Fig. 1 — come from?

The differential rapidity distributions for $\pi^\pm, K^\pm$ and $\Lambda + \Sigma^0$'s from pp collisions, however, show substantial differences as demonstrated in Fig. 12. The experimental data for K^+'s and $\Lambda + \Sigma^0$'s at 160 GeV are taken from Refs. [65] and [66], respectively. Though the π rapidity distributions are roughly comparable in both models, there is a trend for UrQMD to give slightly more pions with decreasing bombarding energy than HSD, whereas in heavy-ion collisions the trend is opposite — HSD gives more pions at low energies than UrQMD, whereas UrQMD gives more pions at high energies[4] (cf. Figs. 2,

---

[4]We will attribute this to the influence of secondary mB scatterings, where more mesons are

3). For K^- mesons the results of both models are comparable at high energies, however, they deviate closer to the K^- production threshold. For K^+ and $\Lambda + \Sigma^0$ both models differ substantially, too. Here HSD gives more K^+ at low energies whereas the UrQMD rapidity distribution is broader at 160 GeV. The Λ yield from pp collisions is also higher from HSD – due to strangeness conservation – and shows distinct peaks in the rapidity distribution closer to target and projectile rapidities at high energies, whereas the UrQMD rapidity distributions for Λ's are narrower and almost peaked at midrapidity. Experimental data [66] – available at 160 GeV – show a minimum at midrapidity giving no strict preference for one of the string fragmentation schemes.

Thus strange quarks are produced more at midrapidity in UrQMD, both for mesons and baryons, whereas in HSD s-quarks are concentrated in mesons at midrapidity and in baryons at larger rapidities. These differences in the elementary differential rapidity spectra explain also the different rapidity distributions from central nucleus-nucleus collisions in Figs. 2 and 3 to a large extent. Presently it is not clear – due to the lack of corresponding experimental data – which fragmentation scheme is 'more realistic'. On the other hand, this comparison sheds some light on the 'systematic' uncertainties in present relativistic transport approaches. These 'systematic' uncertainties have to be kept in mind when attempting to draw conclusions from nucleus-nucleus collisions in comparison to experimental data.

Before closing this Subsection we confront both transport models with the available data on the production cross sections of pions and strange hadrons from pp collisions. In Fig. 13 we show the inclusive π^+, π^-, K^+, K^- and $\Lambda + \Sigma^0$ production cross sections from pp collisions versus the kinetic energy E_{lab}. The solid lines with open triangles show the UrQMD results, the solid line with full squares indicate the HSD results with the strangeness suppression factor γ_s defined by Eq. (2), whereas the dot-dashed lines correspond to $\gamma_s = 0.3$. The experimental data are taken from Refs. [67] (full triangles),

---

produced within UrQMD.

[68] (full and open circles), [69] (open squares) and [70] (stars). The pion cross sections are quite well described by both models; UrQMD gives more π^+ than HSD at low energy in line with the data point from [67], whereas HSD follows more closely the data from Ref. [68]. The inclusive antikaon cross section is well reproduced by both approaches. As already demonstrated in Fig. 12 HSD gives more K^+ and neutral strange hyperons than UrQMD below $E_{lab} \approx 80$ GeV. The neutral hyperon yield from UrQMD (for $E_{lab} \leq 80$ GeV) is more in line with the data, whereas the K^+ yield is slightly underestimated from 10 – 80 GeV. In contrast HSD seems to better reproduce the K^+ cross sections but to overestimate the $\Lambda + \Sigma^0$ yields in pp reactions at lower energies.

The differences in these 'in-put' cross sections are quite sizeable, however, one has to keep in mind that only a single isospin channel is probed in Fig. 13 in comparison to data, whereas in nucleus-nucleus collisions essentially isospin averaged cross sections are of relevance. In fact, both transport models differ in the isospin dependent cross sections for NN collisions, whereas isospin averaged particle yields are more similar. We recall again that strangeness conservation holds explicitly for both transport models with respect to all reactions employed.

B. $\pi^- p$ reactions

We now turn to the elementary pion-nucleon collisions that play a substantial role in secondary meson-baryon collisions. The differential π^+, $K^\pm$ and $\Lambda(+\Sigma^0)$ rapidity distributions from $\pi^- p$ reactions from 2–8 GeV/c laboratory momentum are shown in Fig. 14 for UrQMD (dashed lines) and HSD (solid lines). Also here experimental data are not available for a comparison. Though the total and elastic $\pi^- p$ cross sections are very similar in both models and in line with experimental data (cf. [33,38]), the explicit rapidity distributions for various final states differ by up to a factor of 2-3. This holds true also for the isospin dependent cross sections (e.g. K^+ vs. K^0) that are not probed in nucleus-nucleus collisions due to initial isospin averaging. In general the string model in UrQMD produces substantially more π^+, $K^\pm$ etc. in $\pi + N$ reactions than the LUND model employed in

HSD. Consequently, hadron (including strange meson) production by secondary meson-baryon collisions is sizeably higher in UrQMD than in HSD. This observation clarifies to some extent the higher $\pi^\pm$ yield in Fig. 4 from UrQMD at SPS energies relative to HSD and the experimental data. On the other hand, strangeness production $(K^+, \Lambda + \Sigma^0)$ from pp collisions is much higher in the LUND approach (cf. Fig. 12) than in the FSM (used in UrQMD) such that one might expect the HSD approach to give more kaons and hyperons in central nucleus-nucleus collisions due to a higher initial production. As seen from Figs. 5-7 this expectation does not hold true since in UrQMD the strangeness production from secondary (mB) channels is substantially higher now, which compensates – relative to HSD – for the initially lower strangeness production from NN collisions.

In summary, the dominant differences between HSD and UrQMD for central nucleus-nucleus collisions can be traced back to different string fragmentation schemes for BB and mB strings that lead to substantially different hadron distributions in rapidity as well as isospin. Presently, these string models are not sufficiently controlled by differential experimental data. Furthermore, the string models employed are not tailored to describe the isospin dependence of the elementary cross sections at lower invariant energies $\sqrt{s}$.

C. pp versus central AA reactions

In order to explore the main physics from central AA reactions it is instructive to have a look at the various particle multiplicities relative to pp collisions as a function of bombarding energy. To this aim we show in Fig. 15 the total multiplicities of π^+, K^+ and K^- (i.e. the 4π yields) from central $Au + Au$ (at AGS) or $Pb + Pb$ (at SPS) collisions in comparison to the total multiplicities from pp collisions versus the kinetic energy per particle E_{lab}. The solid lines with full triangles and squares show the UrQMD (l.h.s.) and HSD results (r.h.s.) for AA collisions, respectively, while the dotted lines with open triangles and squares correspond to the pp multiplicities calculated within UrQMD (l.h.s.) and HSD (r.h.s.). The multiplicities from pp reactions in Fig. 15 have been multiplied by a factor of 350/2 which corresponds to the average number of participants A_{part} in the heavy-

ion reactions for the centrality class considered divided by the number of participants in the pp reaction. We mention, that the comparison at lower bombarding energies of 2–4 A·GeV has to be taken with some care due to the different influence of Fermi motion - in case of AA reactions - on the production of pions and $K^{\pm}$ mesons.

The general trend from both transport approaches is quite similar: we observe a slight absorption of pions at lower bombarding energy and a relative enhancement of pion production in heavy-ion collisions above about 10 A·GeV. Kaons and antikaons from AA collisions are always enhanced in central reactions relative to scaled pp multiplicities. This enhancement is more pronounced within UrQMD than in HSD due to the larger cross sections employed in πN secondary reactions as demonstrated in the previous Subsection.

VI. SUMMARY

In this work we have performed a systematic analysis of hadron production in central $Au + Au$ or $Pb + Pb$ collisions from SIS to SPS energies within the HSD (with and without potentials) and UrQMD transport approaches in comparison to the experimental data available. We find that both transport approaches — which are based on quite different initial ingredients — roughly give comparable results for the different $p, \pi^{\pm}, K^{\pm}$ and hyperon distributions in a wide energy regime from 2 – 160 A·GeV. It is remarkable that the cascade mode of HSD (which operates by default in the potential mode) gives to a large extent comparable results for strangeness production as the UrQMD cascade. This observation suggests that — inspite of the different elementary 'input' cross sections — the systems might reach approximate chemical equilibrium. This is a prerequisite for an analysis within statistical models [35,62,71]. In fact, the channel decomposition of strangeness production chains in both models are quite different (cf. Fig. 10) since the degrees of freedom (hadron resonances and strings) substantially differ for collisions at hadron-hadron collision energies around 2-3 GeV in the region of string thresholds.

We have found that at SPS energies HSD and UrQMD quite well reproduce the experimental data for K^- and $\Lambda + \Sigma^0$ rapidity distributions at midrapidity as well as the

23

4π yields. At 20 A·GeV both models agree very well among each other for all hadrons. This provides rather solid predictions for the future GSI heavy-ion program [41]. At AGS energies ($\leq$ 11 A·GeV) the K^+ yield is slightly overestimated by UrQMD (except of 10.7 A·GeV), whereas HSD underestimats kaon production at the upper AGS energies (especially with baryon potentials included). The K^- and $\Lambda + \Sigma^0$ data are reasonably described by both models. We have found also that HSD and UrQMD differ in the pion multiplicities — at lower AGS energies the UrQMD model gives slightly less pions than HSD (with/without potential), but both models overpredict the midrapidity data (except UrQMD at 2 A·GeV). At SPS energies the tendency turns around: UrQMD gives more pions than HSD, such that HSD is now in a better agreement with the experimental data. These differences between the transport approaches could be traced back to a large extent to different string fragmentation schemes which presently are insufficiently controlled by experimental data at the energies of interest here.

The excitation functions of pions, kaons and antikaons from central $Au + Au$ (or $Pb + Pb$) collisions relative to scaled pp reactions from the two transport models are very similar: both approaches give an absorption of pions at lower bombarding energy and a relative increase of pion production for $E_{lab} > 10$ A·GeV. Kaons and antikaons from AA collisions are enhanced in central reactions relative to scaled pp collisions at all energies by a factor of ≥ 2.

We have found that the failure of both models to reproduce the experimental excitation function for the K^+/π^+ ratio in central nucleus-nucleus collisions — which might suggest the presence of a different state of hadronic matter in the early phase of these collisions — is not primarily due to an underestimation of strangeness production. Our systematic study in comparison to the most recent data from the NA49 Collaboration demonstrates that this failure is mainly due to an inadequate description of pion dynamics. We attribute this to the fact that the pions in both transport models are treated as 'free' on-shell particles, i.e. with their vacuum properties and δ-like spectral functions in mass. On the other hand, lattice QCD as well as effective Lagrangian models indicate an increase of the pion mass with temperature and density. Furthermore, the pion spectral function should

become broad in the medium due to the interactions. All these medium modifications have not been included in the calculations presented in the work. Thus the overestimation of the pion yields could be a signature for a chiral symmetry restoration which might occur at the high baryon/meson densities achieved in relativistic heavy-ion collisions. Including the medium effects for pions and all strange particles simultaneously in a consistent way in an 'off-shell transport approach' [72] could provide a more conclusive interpretation of the experimental data. This, however, requires a precise knowledge about the momentum and density dependence of the hadron self-energies in a wide energy regime and full off-shell transition matrix elements [72]. Such a program is clearly beyond the scope of our present study.

Another problem of the transport approaches used here is that detailed balance is not implemented for $n \leftrightarrow m$ transitions with $n, m > 2$ [36]. Thus multi-particle collisions might change the dynamical picture accordingly and lead to 'shorter' chemical equilibration times [60,73,74]. In fact, the importance of $3 \leftrightarrow 2$ transitions has been demonstrated in the extended HSD transport approach in Ref. [60] for antibaryon reproduction by meson fusion for $A + A$ collisions at the AGS and SPS. In order to achieve a more conclusive answer from transport studies multiparticle interactions will have to be included in future generations of transport codes.

What to conclude from the detailed comparisons presented in this work? Coming back to the question raised in the introduction about common failures in comparison to related experimental data, we can quote an insufficient accuracy in the description of the pion degrees of freedom by both transport models. Does this provide a signal for 'new physics' in view of a QGP? The answer of the authors to this question with respect to the experimental observables studied is: no! As discussed above, the 'systematic uncertainties' in the 'on-shell' transport approaches are within the range of the deviations seen in comparison to the data or even larger. Furthermore, the question raised in the title of this paper – anything strange with strangeness? – also has to be answered with 'most likely not'!

ACKNOWLEDGEMENT

REFERENCES

[1] J. W. Harris and B. Müller, Annu. Rev. Nucl. Part. Sci. **46**, 71 (1996).

[2] E. V. Shuryak, Rev. Mod. Phys. **65**, 1 (1993).

[3] Quark Matter'99, Nucl. Phys. A **661**, 1c (1999).

[4] U. Heinz, M. Jacob, 'Evidence for a New State of Matter: An Assessment of the result from the CERN Lead Beam Programme', CERN Press Office (2000); nucl-th/0002042.

[5] S. A. Bass, M. Gyulassy, H. Stöcker, and W. Greiner, J. Phys. G **25**, R1 (1999).

[6] Quark Matter'01, Nucl. Phys. A **698**, 1c (2001).

[7] J. D. Bjorken, Phys. Rev. D **27**, 140 (1983).

[8] K. Geiger and B. Müller, Nucl. Phys. B **369**, 600 (1992).

[9] K. Geiger, Phys. Rep. **258**, 237 (1995).

[10] X.-N. Wang, Phys. Rep. **280**, 287 (1997).

[11] R. Baier, Y. L. Dokshitzer, A. H. Mueller, and D. Schiff, Phys. Rev. C **58**, 1706 (1998).

[12] J. Ruppert, G. C. Nayak, D. D. Dietrich, H. Stöcker, and W. Greiner, Phys. Lett. B **520**, 233 (2001).

[13] S. A. Bass, M. Hofmann, M. Bleicher, L. Bravina, E. Zabrodin, H. Stöcker, and W. Greiner, Phys. Rev. C **60**, 021901 (1999).

[14] S. A. Bass, M. Bleicher, W. Cassing et al., Nucl. Phys. A **661**, 205c (1999).

[15] Zi-Wei Lin, S. Pal, C.M. Ko, Bao-An Li, and Bin Zhang, Phys. Rev. C **64**, 011902 (2001); Nucl. Phys. A **698**, 375 (2002); Bin Zhang, C. M. Ko, Bao-An Li, Zi-Wei Lin, and S. Pal, Phys. Rev. C **65**, 034904 (2002).

[16] P. F. Kolb, U. Heinz, P. Huovinen, K. J. Eskola, and K. Tuominen, Nucl. Phys. A **696**, 197 (2001).

[17] G. E. Brown and M. Rho, Phys. Rev. Lett. **66**, 2720 (1991).

[18] V. Koch, Int. J. Mod. Phys. E **6**, 203 (1997).

[19] J. V. Steele, H. Yamagishi, and I. Zahed, Phys. Lett. B **384**, 255 (1996); Phys. Rev. D **56**, 5605 (1997).

[20] B. Friman, W. Nörenberg and V. D. Toneev, Eur. Phys. J. A **3**, 165 (1998).

[21] W. Cassing, E. L. Bratkovskaya, S. Juchem, Nucl. Phys. A **674**, 249 (2000).

[22] M. Gaździcki and D. Röhrich, Z. Phys. C **65**, 215 (1995); M. Gaździcki and M. I. Gorenstein, Acta Phys. Polon. B **30**, 2705 (1999).

[23] S.V. Afanasiev et al. (NA49 Collab.), nucl-ex/0205002; to be published in Phys. Rev. C.

[24] A. Mischke et al. (NA49 Collab.), J. Phys. G. **28**, 1761 (2002).

[25] A. Mischke et al. (NA49 Collab.), nucl-ex/0209002, to be published in Nucl. Phys. A.

[26] The NA49 Collaboration, Addendum-10 to Proposal CERN/SPSC/P264, 'Progress Report and Beam Request for 2002'.

[27] W. Cassing and E. L. Bratkovskaya, Phys. Rep. **308**, 65 (1999).

[28] H. Stöcker and W. Greiner, Phys. Rep. **137**, 277 (1986).

[29] G. F. Bertsch and S. Das Gupta, Phys. Rep. **160**, 189 (1988).

[30] W. Cassing, V. Metag, U. Mosel, and K. Niita, Phys. Rep. **188**, 363 (1990).

[31] C. M. Ko and G. Q. Li, J. Phys. G **22**, 1673 (1996).

[32] F. Wang, H. Liu, H. Sorge, N. Xu, and J. Yang, Phys. Rev. C **61**, 064904 (2000).

[33] J. Geiss, W. Cassing, and C. Greiner, Nucl. Phys. A **644**, 107 (1998).

[34] H. Weber, E.L. Bratkovskaya, and H. Stöcker, Phys. Lett. B **545**, 285 (2002).

[35] P. Braun-Munzinger, J. Cleymans, H. Oeschler and K. Redlich, Nucl. Phys. A **697**, 902 (2002).

[36] M. Belkacem, M. Brandstetter, S.A. Bass et al., Phys. Rev. C **58**, 1727 (1998); L.V. Bravina, M.I. Gorenstein, M. Belkacem et al., Phys. Lett. B **434**, 379 (1998); L.V. Bravina, M. Brandstetter, M.I. Gorenstein et al., J. Phys. G **25**,351 (1999); L.V. Bravina, E.E. Zabrodin, M.I. Gorenstein et al., Phys. Rev. C **60**, 024904 (1999).

[37] E. L. Bratkovskaya, W. Cassing, C. Greiner, M. Effenberger, U. Mosel and A. Sibirtsev, Nucl. Phys. A **675**, 661 (2000).

[38] S.A. Bass, M. Belkacem, M. Bleicher, M. Brandstetter, L. Bravina, C. Ernst, L. Gerland, M. Hofmann, S. Hofmann, J. Konopka, G. Mao, L. Neise, S. Soff, C. Spieles, H. Weber, L.A. Winckelmann, H. Stöcker, W. Greiner, Ch. Hartnack, J. Aichelin, and N. Amelin, Prog. Part. Nucl. Phys. **42**, 279 (1998).

[39] M. Bleicher, E. Zabrodin, C. Spieles, S.A. Bass, C. Ernst, S. Soff, L. Bravina, M. Belkacem, H. Weber, H. Stöcker, and W. Greiner, J. Phys. G **25**, 1859 (1999).

[40] W. Ehehalt and W. Cassing, Nucl. Phys. A **602**, 449 (1996).

[41] 'An International Accelerator Facility for Beams of Ions and Antiprotons', http://www.gsi.de/GSI-Future/cdr/.

[42] C. Caso et al., (Review of Particle Properties), Eur. Phys. J. C **15**, 1 (2000).

[43] L. A. Kondratyuk, M. Krivoruchenko, N. Bianchi, E. De Sanctis, and V. Muccifora, Nucl. Phys. A **579**, 453 (1994).

[44] R. Rapp and J. Wambach, Adv. Nucl. Phys. **25**, 1 (2000).

[45] N. Bianchi at al., Phys. Lett. B **309**, 5 (1993); B **325**, 333 (1994); Phys. Rev. C **54**, 1688 (1996).

[46] B. Nilsson-Almqvist and E. Stenlund, Comp. Phys. Comm. **43**, 387 (1987); B. An-

derson, G. Gustafson and Hong Pi, Z. Phys. C **57**, 485 (1993).

[47] J. Schwinger, Phys. Rev. **83**, 664 (1951).

[48] J. Schwinger, J. Math Phys. **2**, 407 (1961); L. Kadanoff and G. Baym, Quantum Statistical Mechanics (W.A. Benjamin, New York, 1962).

[49] B. Holzman et al.(E917 Collab.), Nucl. Phys. A **698**, 643 (2002).

[50] C.E. Copper et al. (NA49 collab.), Nucl. Phys. A **661**, 362c (1999).

[51] H. Appelshäuser et al.(NA49 Collab.), Phys. Rev. Lett. **82**, 2471 (1999).

[52] H. Weber, E.L. Bratkovskaya, and H. Stöcker, nucl-th/0205032, Phys. Rev. C (2002), in press.

[53] L. Ahle et al. (E866 and E917 Collab.), Phys. Lett. B **476**, 1 (2000); Phys. Lett. B **490**, 53 (2000).

[54] W.-C. Chang et al. (E917 Collab.), nucl-ex/99040110; Proceedings of the 15Th Winter Workshop on Nuclear Dynamics, ParkCity, UT, Janyary 1999.

[55] Y. Akiba et al. (E866 Collab.), Nucl. Phys. A **610**, 139c (1996).

[56] L. Ahle et al. (E877 Collab.), Phys. Rev. C **57**, R466 (1998); J. Barrette et al. (E877 Collab.), Phys. Rev. C **63**, 014902 (2001).

[57] S. Ahmad et al. (E891 Collab.), Phys. Lett. B **382**, 35 (1996); C. Pinkenburg et al. (E866 Collab.), Nucl. Phys. A **698**, 495c (2002).

[58] S. Albergo et al., (E896 Collab.), Phys. Rev. Lett. **88**, 062301 (2002).

[59] A. B. Larionov, W. Cassing, S. Leupold, and U. Mosel, Nucl. Phys. A **696**, 747 (2001).

[60] W. Cassing, Nucl. Phys. A **700**, 618 (2002).

[61] F. Antiori at al. (WA97 Collab.), Nucl. Phys. A **661**, 130c (1999).

[62] D. Zschiesche, S. Schramm, J. Schaffner-Bielich, H. Stöcker, and W. Greiner, nucl-th/0209022.

[63] D. B. Kaplan and A. E. Nelson, Phys. Lett. B **175**, 57 (1986); G. E. Brown, C. M. Ko, Z. G. Wu, and L. H. Xia, Phys. Rev. C **43**, 1881 (1991); T. Waas, N. Kaiser, and W. Weise, Phys. Lett. B **365**, 12 (1996).

[64] S. Soff, S.A. Bass, M. Bleicher et al., Phys. Lett **B 471**, 89 (1999).

[65] C. Höhne et al., (NA49 Collab.), Nucl. Phys. A **661**, 485c (1999).

[66] T. Šuša at al., (NA49 Collab.), Nucl. Phys. A **698**, 491c (2002).

[67] Landolt-Börnstein 1988 *New Series*, ed. H. Schopper, I/12.

[68] M. Antinucci et al., Lett. al Nuovo Cimento, **6**, 121 (1973).

[69] M. Gaździcki and D. Röhrich, Z. Phys. C **71**, 55 (1996).

[70] J. Bächler et al. (NA49 Collab.), Nucl. Phys. A **661**, 45 (1999).

[71] D. Hahn and H. Stöcker, Nucl. Phys. A **476**, 718 (1988).

[72] W. Cassing, S. Juchem, Nucl. Phys. A **665**, 377 (2000); Nucl. Phys. A **672**, 417 (2000); Nucl. Phys. A **677**, 445 (2000).

[73] R. Rapp and E. V. Shuryak, Phys. Rev. Lett. **86**, 2980 (2001).

[74] C. Greiner and S. Leupold, J. Phys. G **27**, L95 (2001).
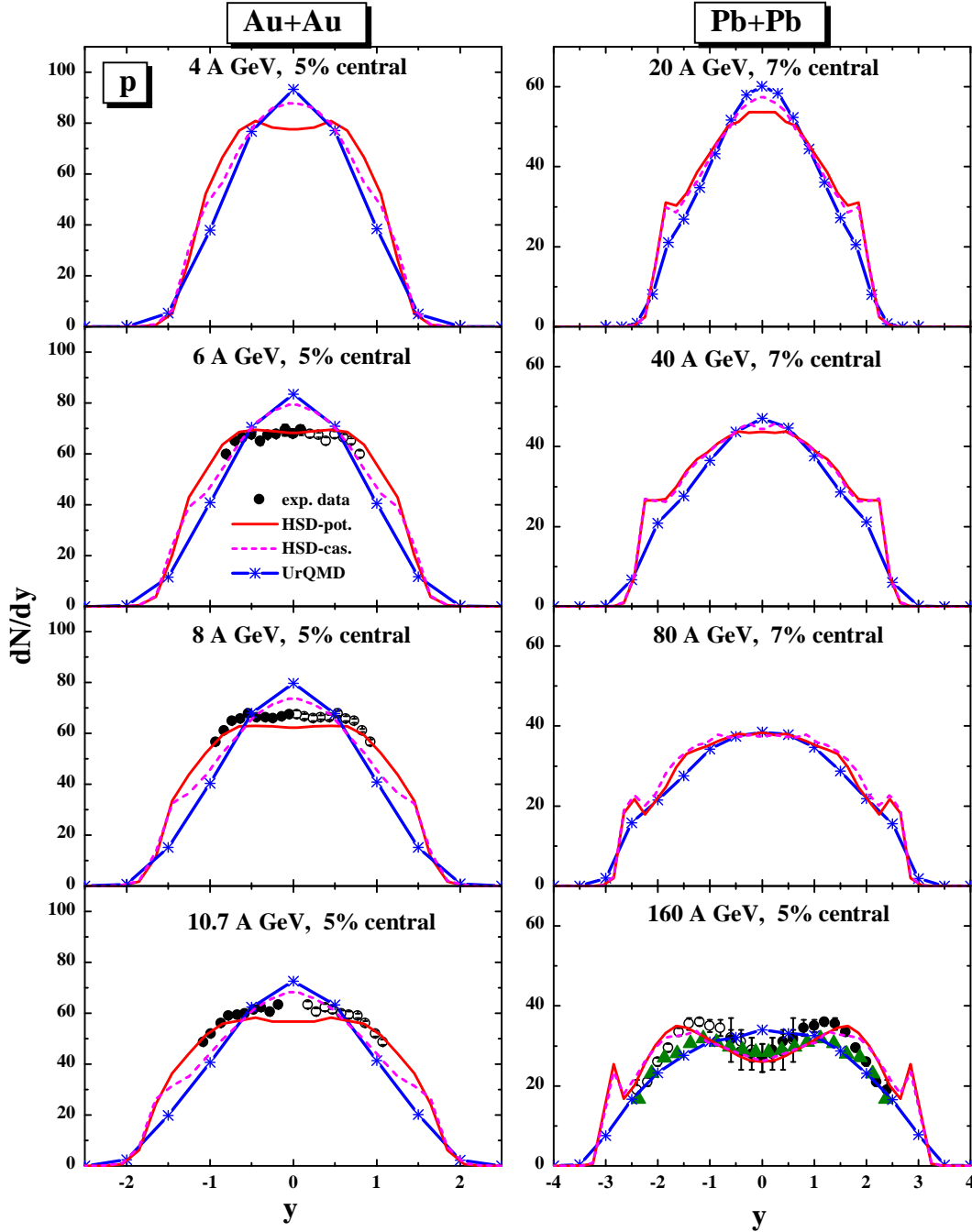
FIG. 1. The rapidity distributions for protons from 5% (4, 6, 8, 10.7 and 160 A·GeV) and 7% central (20, 40, 80 A·GeV) $Au + Au$ (AGS) and $Pb + Pb$ (SPS) collisions at 4–160 A·GeV. The experimental data at 4, 6, 8, 10.7 A·GeV have been taken from Ref. [49] (circles), at 160 A·GeV from [50] (triangles) and from [51] (circles). The full symbols correspond to the measured data, whereas the open symbols are the data reflected at midrapidity. The solid lines with stars show the results from the UrQMD calculations while the solid and dashed lines stem from the HSD approach with and without potentials, respectively.
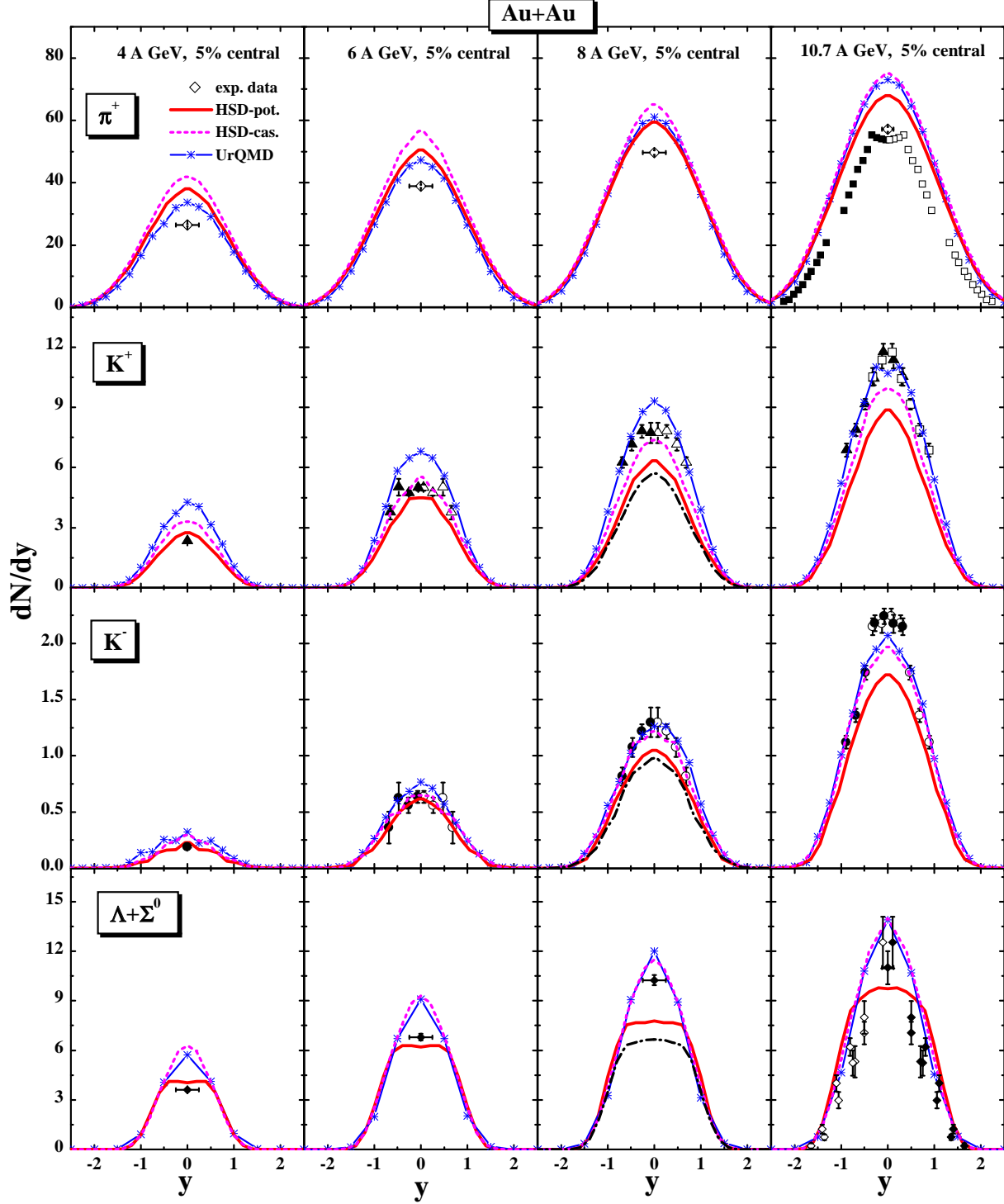
FIG. 2. The rapidity distributions for π^+, K^+, K^- and $\Lambda + \Sigma^0$'s from 5% central $Au + Au$ collisions at 4–10.7 A·GeV in comparison to the experimental data from Refs. [53–58]. The thin solid lines with stars show the results from the UrQMD calculations while the thick solid and dashed lines stem from the HSD approach with and without potentials, respectively.
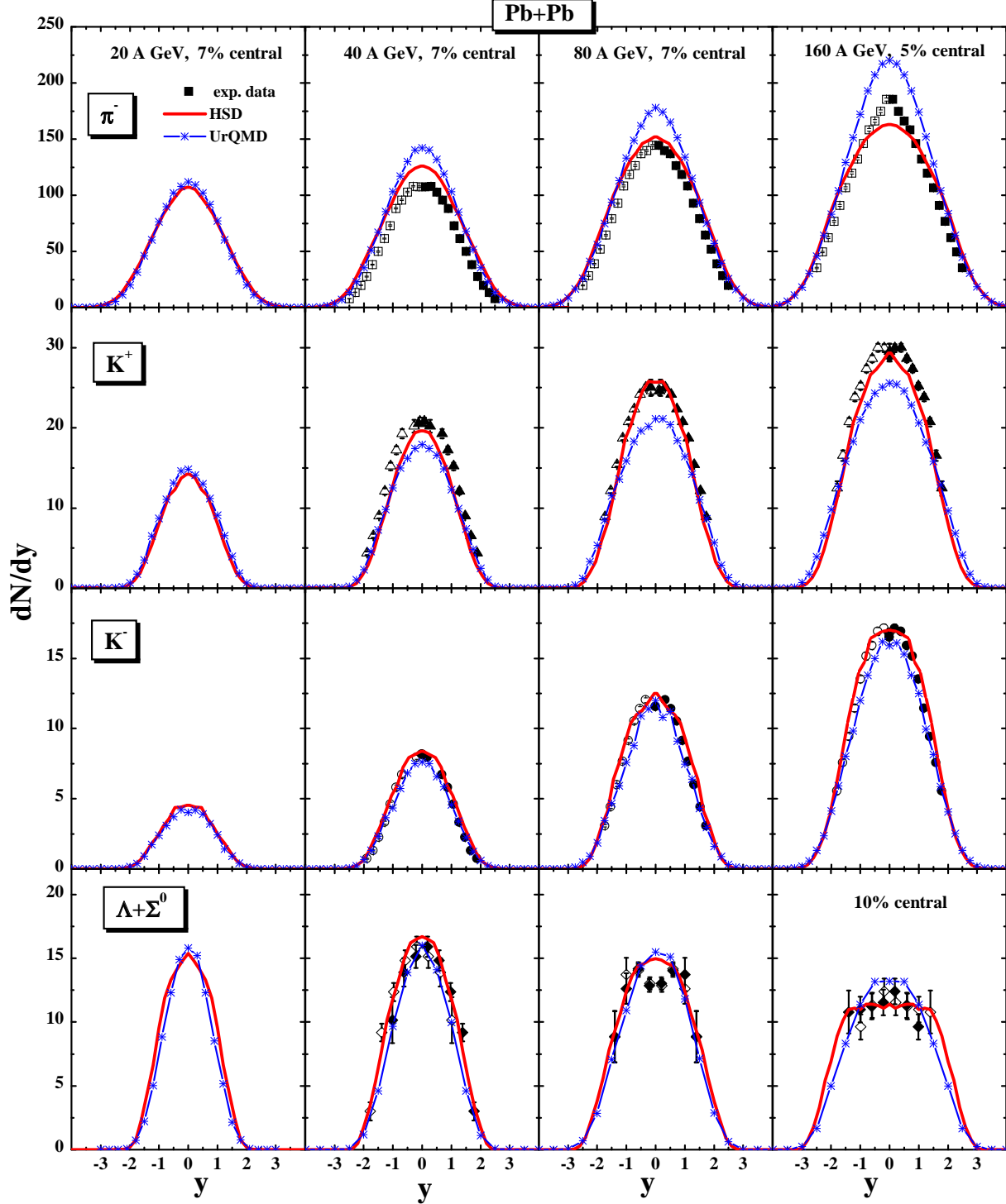
FIG. 3. The rapidity distributions for π^-, K^+, K^- and $\Lambda + \Sigma^0$'s from 5% (160 A·GeV), 7% (20, 40 and 80 A·GeV) or 10% central ($\Lambda + \Sigma^0$ at 160 A·GeV) $Pb + Pb$ collisions at 20–160 A·GeV in comparison to the experimental data from Refs. [23–25]. The solid lines with stars show the results from the UrQMD calculations while the thick solid and dashed lines stem from the HSD approach with and without potentials, respectively.
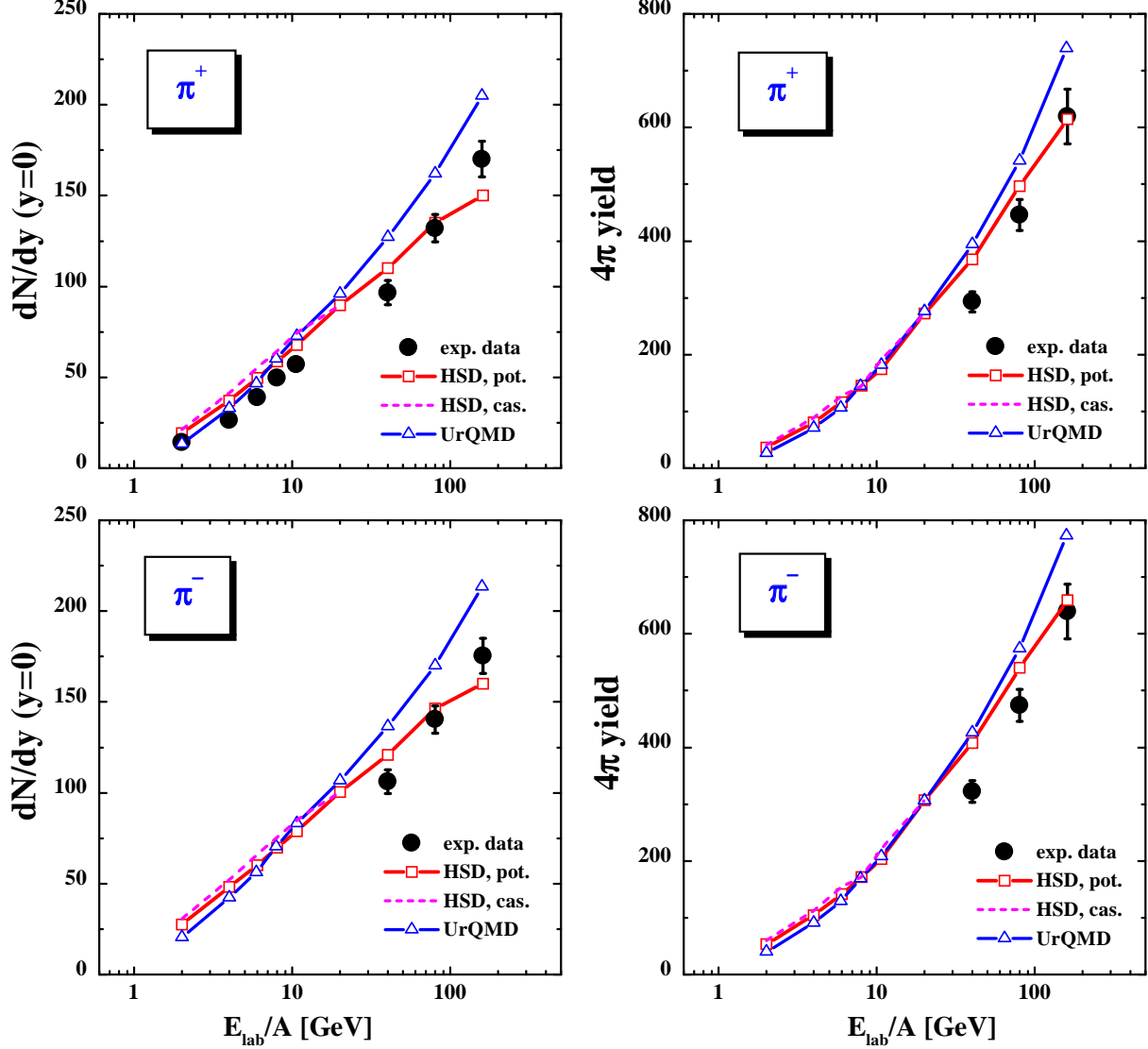
FIG. 4. The excitation function of π^+ (upper plots) and π^- (lower plots) yields from 5% (AGS energies and 160 A·GeV) or 7% central (20, 40 and 80 A·GeV) $Au+Au$ (AGS) or $Pb+Pb$ (SPS) collisions in comparison to the experimental data from Refs. [53,23] for midrapidity (left column) and rapidity integrated yields (right column). The solid lines with open triangles show the results from the UrQMD calculations while the solid lines with open squares and dashed lines stem from the HSD approach with and without potentials, respectively.
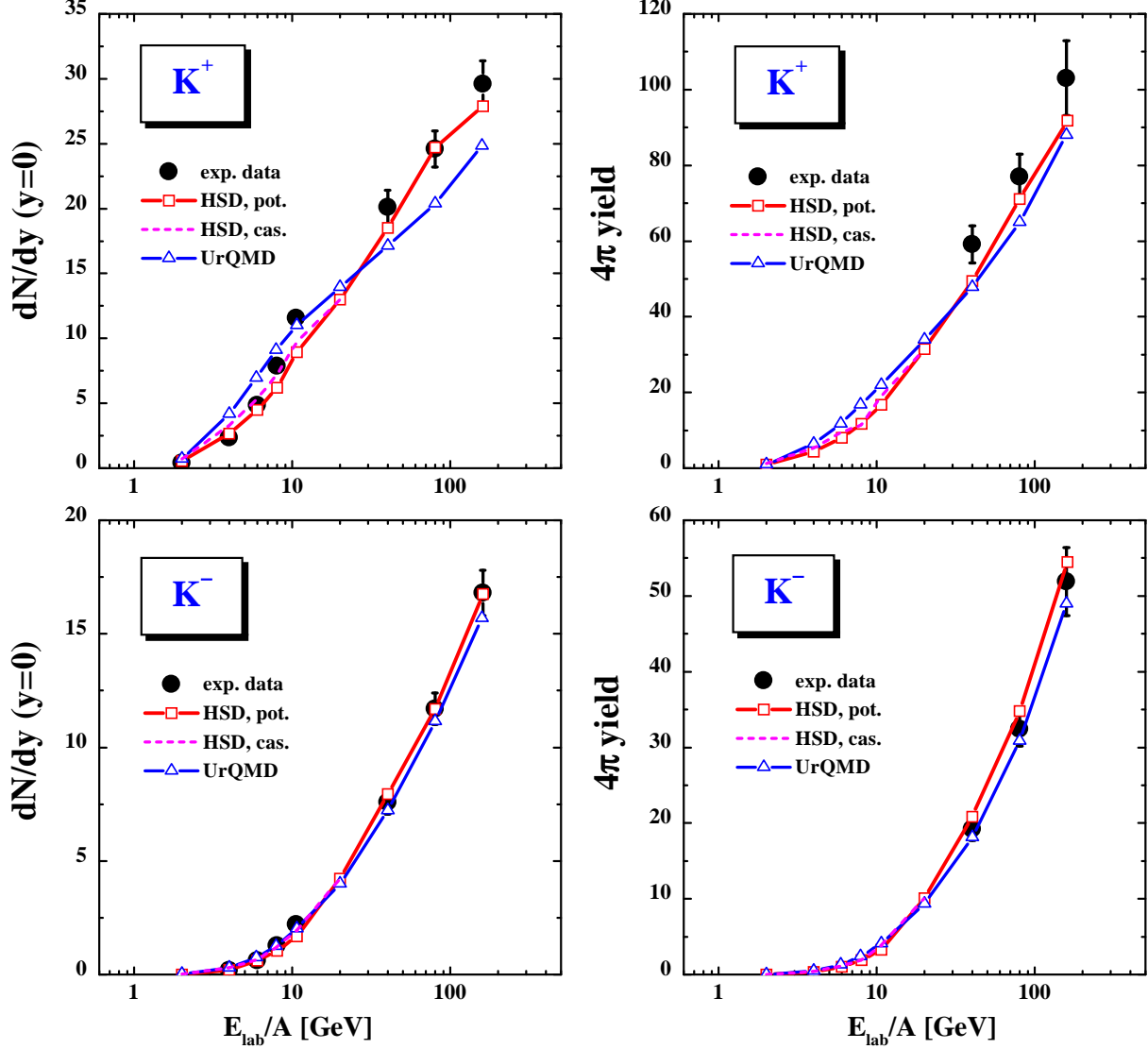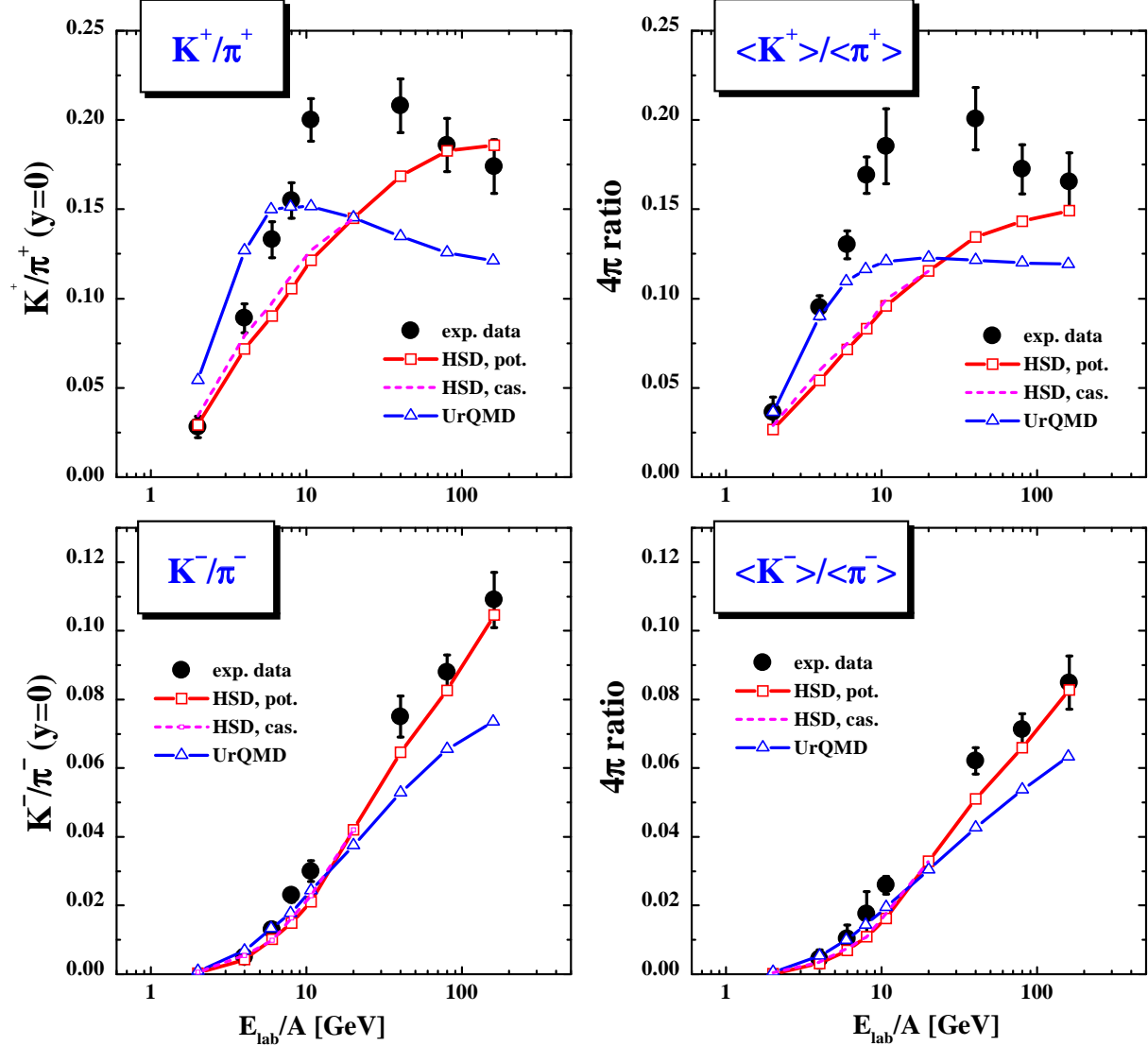
FIG. 5. The excitation function of K^+ (upper plots) and K^- (lower plots) yields from 5% (AGS energies and 160 A·GeV) or 7% central (20, 40 and 80 A·GeV) $Au+Au$ (AGS) or $Pb+Pb$ (SPS) collisions in comparison to the experimental data from Refs. [53,23] for midrapidity (left column) and rapidity integrated yields (right column). The solid lines with open triangles show the results from the UrQMD calculations while the solid lines with open squares and dashed lines stem from the HSD approach with and without potentials, respectively.
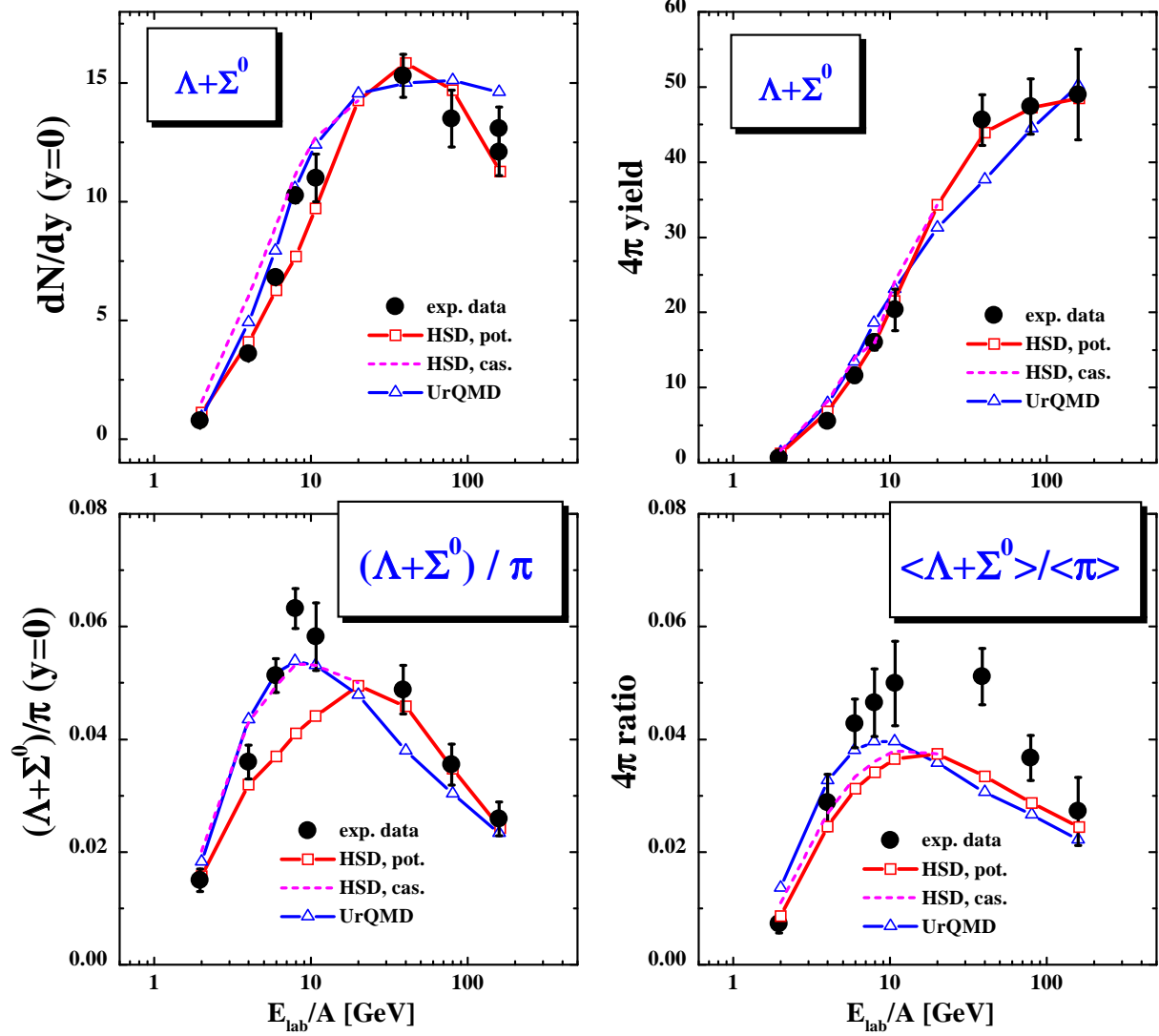
FIG. 6. The excitation function of the K^+/π^+ (upper plots) and K^-/π^- (lower plots) ratios from 5% (AGS energies and 160 A·GeV) or 7% central (20, 40 and 80 A·GeV) $Au + Au$ (AGS) or $Pb + Pb$ (SPS) collisions in comparison to the experimental data from Refs. [53,23] for midrapidity (left column) and rapidity integrated yields (right column). The solid lines with open triangles show the results from the UrQMD calculations while the solid lines with open squares and dashed lines stem from the HSD approach with and without potentials, respectively.
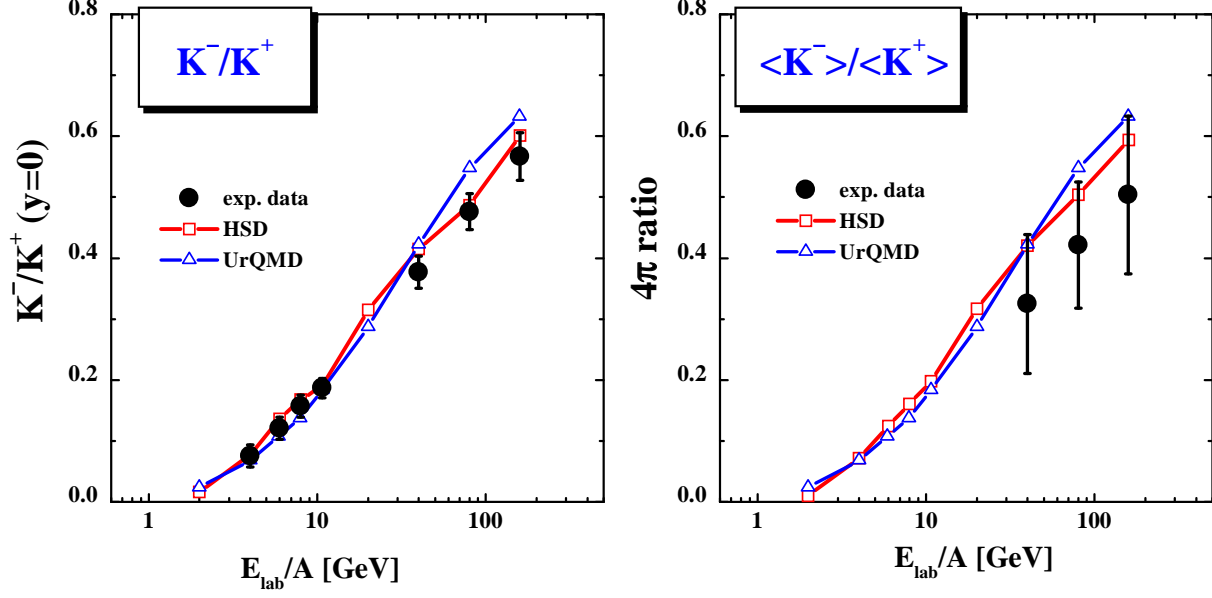
FIG. 7. The excitation function of the $\Lambda + \Sigma^0$ yields and $(\Lambda + \Sigma^0)/\pi$ ratio from 5% (AGS energies), 7% (20, 40 and 80 A·GeV) or 10% central (160 A·GeV) $Au + Au$ (AGS) or $Pb + Pb$ (SPS) collisions in comparison to the experimental data from Refs. [24,25,57,61] for midrapidity (left column) and rapidity integrated yields (right column). The solid lines with open triangles show the results from the UrQMD calculations while the solid lines with open squares and dashed lines stem from the HSD approach with and without potentials, respectively.
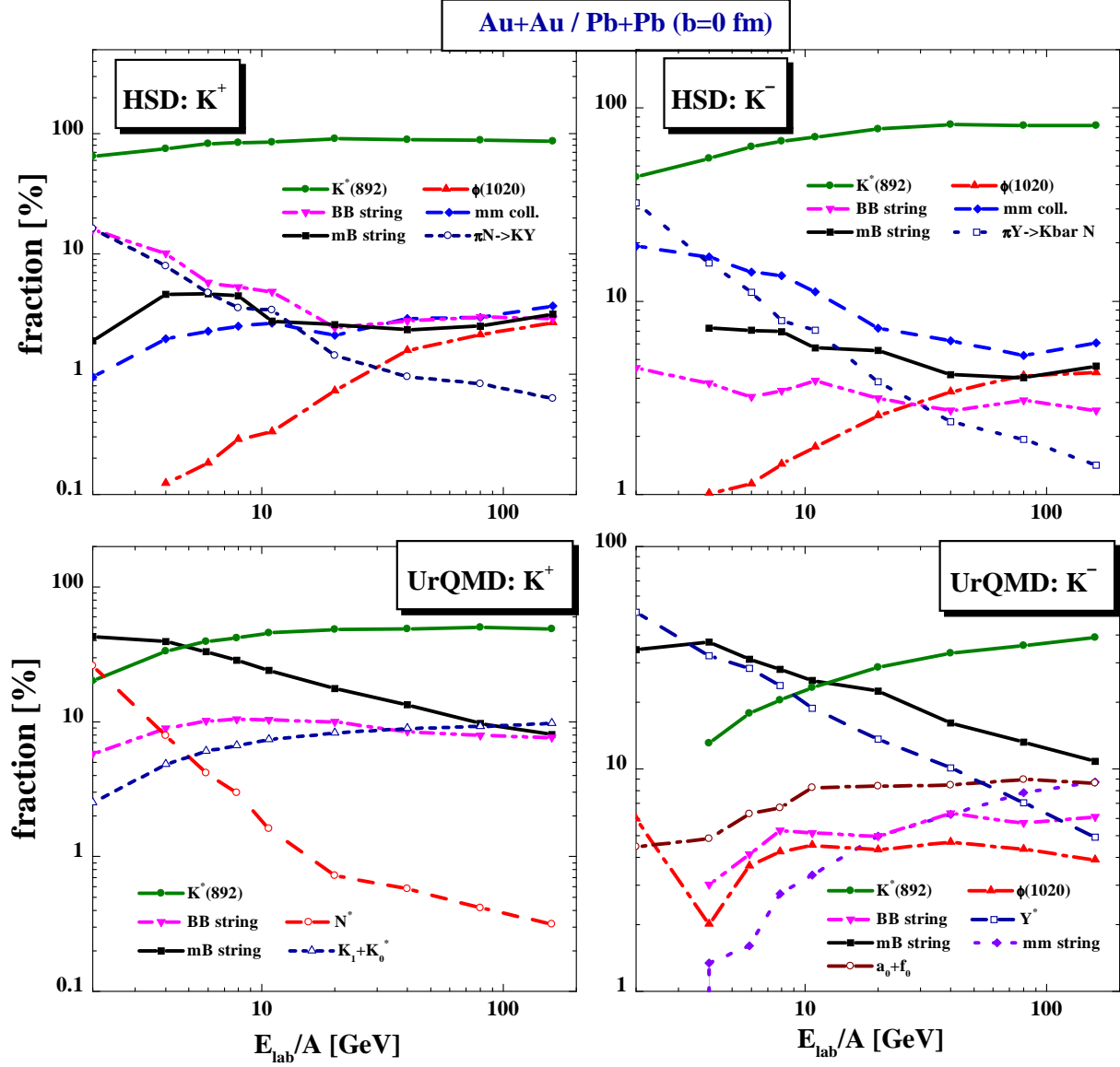
FIG. 8. The excitation function of the K^-/K^+ ratio from 5% (AGS energies and 160 A·GeV) or 7% central (20, 40 and 80 A·GeV) $Au + Au$ (AGS) or $Pb + Pb$ (SPS) collisions in comparison to the experimental data from Refs. [53,23] for midrapidity (left column) and rapidity integrated yields (right column). The solid lines with open triangles show the results from the UrQMD calculations while the solid lines with open squares stem from the HSD approach with potentials.

FIG. 9. The excitation function of s and $\bar{s}$ production from central $Au+Au$ (AGS) or $Pb+Pb$ (SPS) collisions at impact parameter $b = 0$ for HSD (l.h.s.) and UrQMD (r.h.s.) as appearing in mesons or baryons (antibaryons). The solid (dashed) lines with full (open) squares and circles indicate the number of s-quarks ($\bar{s}$-quarks) in baryons (antibaryons) and mesons, respectively.

FIG. 10. The excitation function of the channel decomposition for K^+ and K^- from HSD (upper part) and UrQMD (lower part) from central $Au + Au$ (AGS) or $Pb + Pb$ (SPS) collisions at impact parameter $b = 0$.
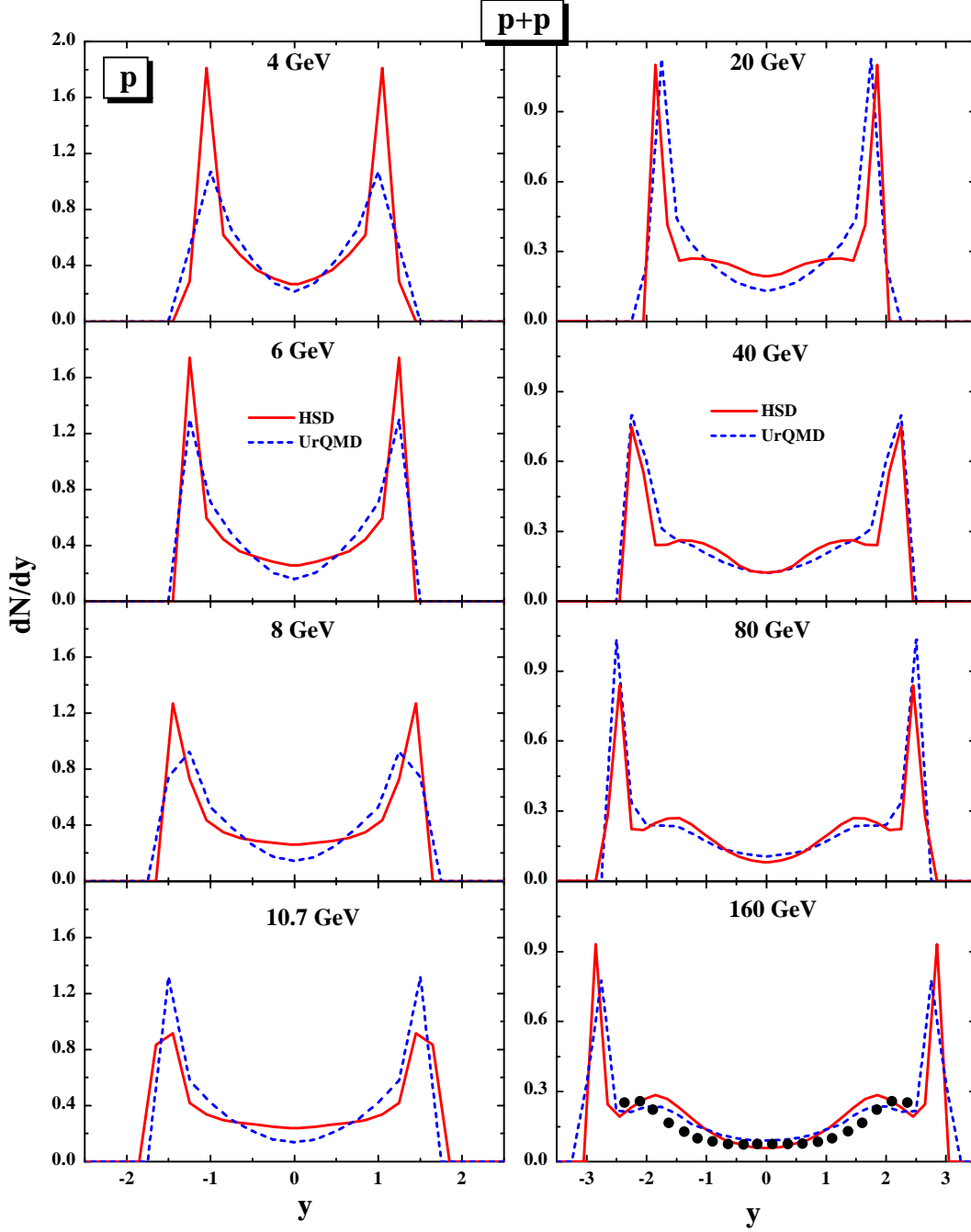
FIG. 11. The rapidity distribution of protons from *pp* collisions at 4–160 GeV as calculated within HSD (solid lines) and UrQMD (dashed lines). The experimental data at 160 GeV are taken from Ref. [50].
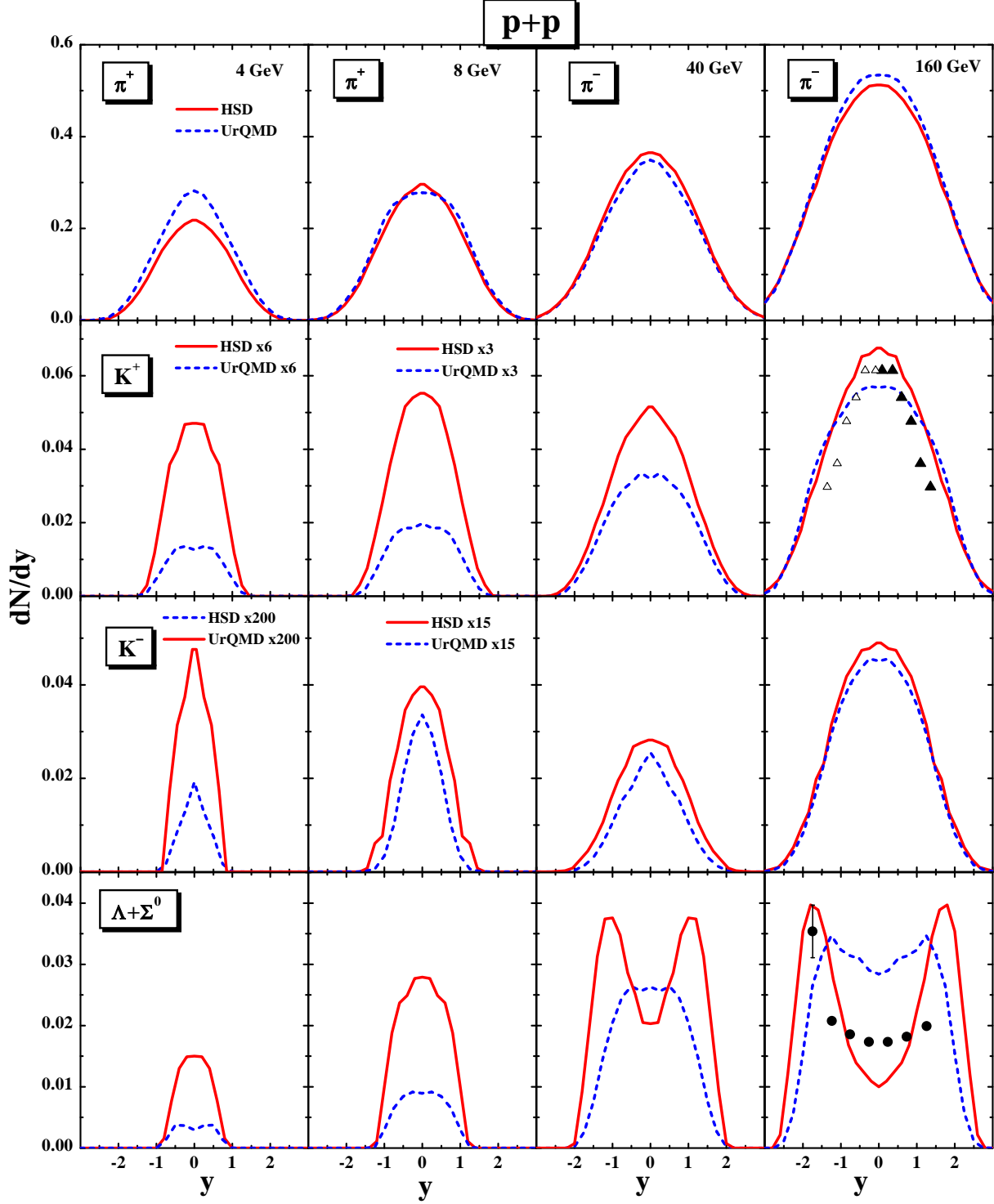
FIG. 12. The rapidity distribution of π^+, K^+, K^- and $\Lambda + \Sigma^0$'s from pp collisions at 4–160 GeV as calculated within HSD (solid lines) and UrQMD (dashed lines). The K^+ rapidity distributions from HSD and UrQMD at 4 and 8 GeV are scaled by factors of 6 and 3 while the K^- rapidity distributions are scaled by factors of 200 and 15, respectively. The experimental data for K^+'s and $\Lambda + \Sigma^0$'s at 160 GeV are taken from Refs. [65] and [66].
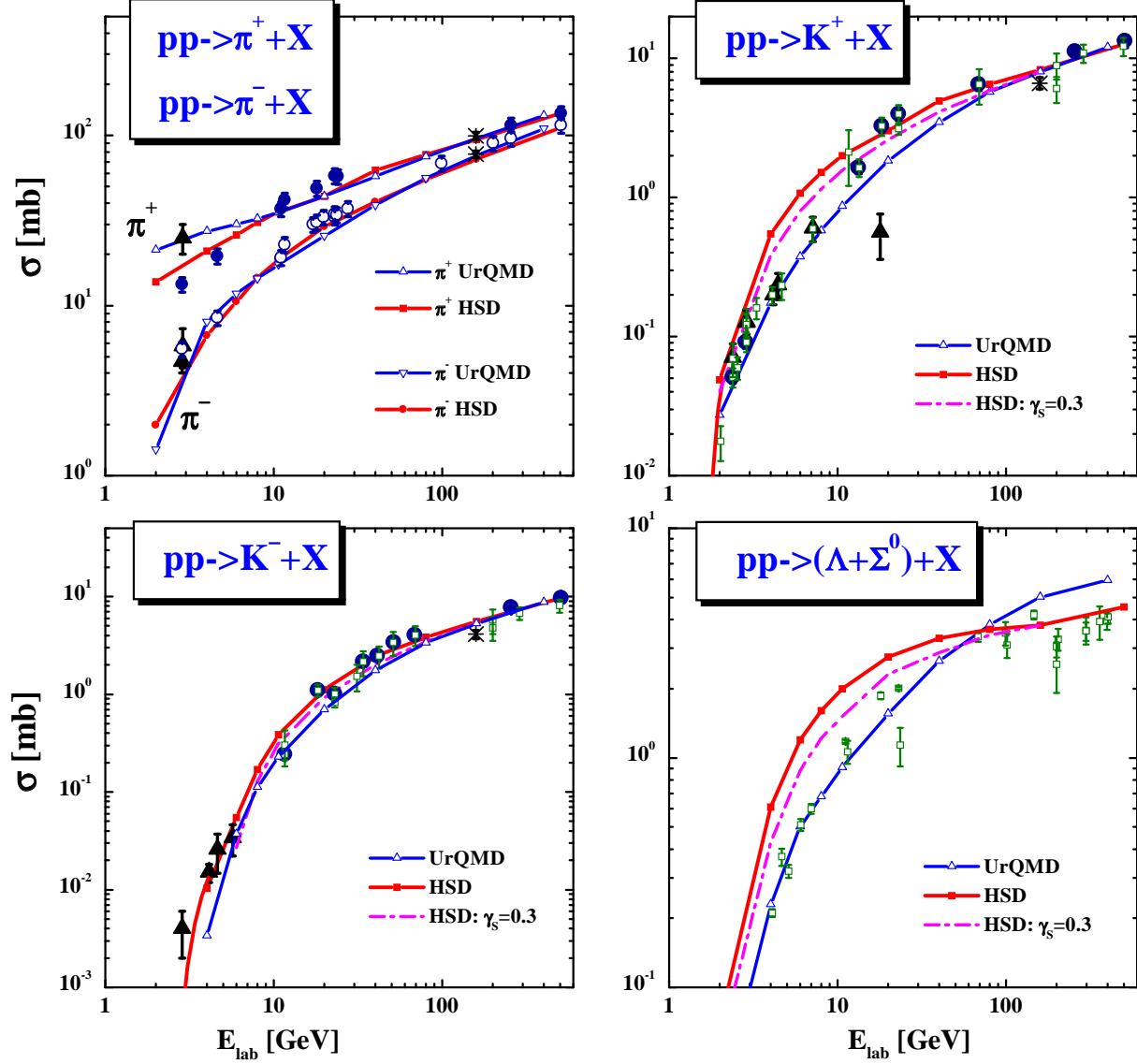
FIG. 13. The inclusive π^+, π^-, K^+, K^- and $\Lambda + \Sigma^0$ production cross sections from pp collisions versus kinetic energy E_{lab}. The solid lines with open triangles show the UrQMD results, the solid line with full squares indicate the HSD results with γ_s defined by Eq. (2), whereas the dot-dashed lines correspond to the $\gamma_s = 0.3$. The exp. data are taken from Refs. [67] (full triangles), [68] (full and open circles), [69] (open squares) and [70] (stars).
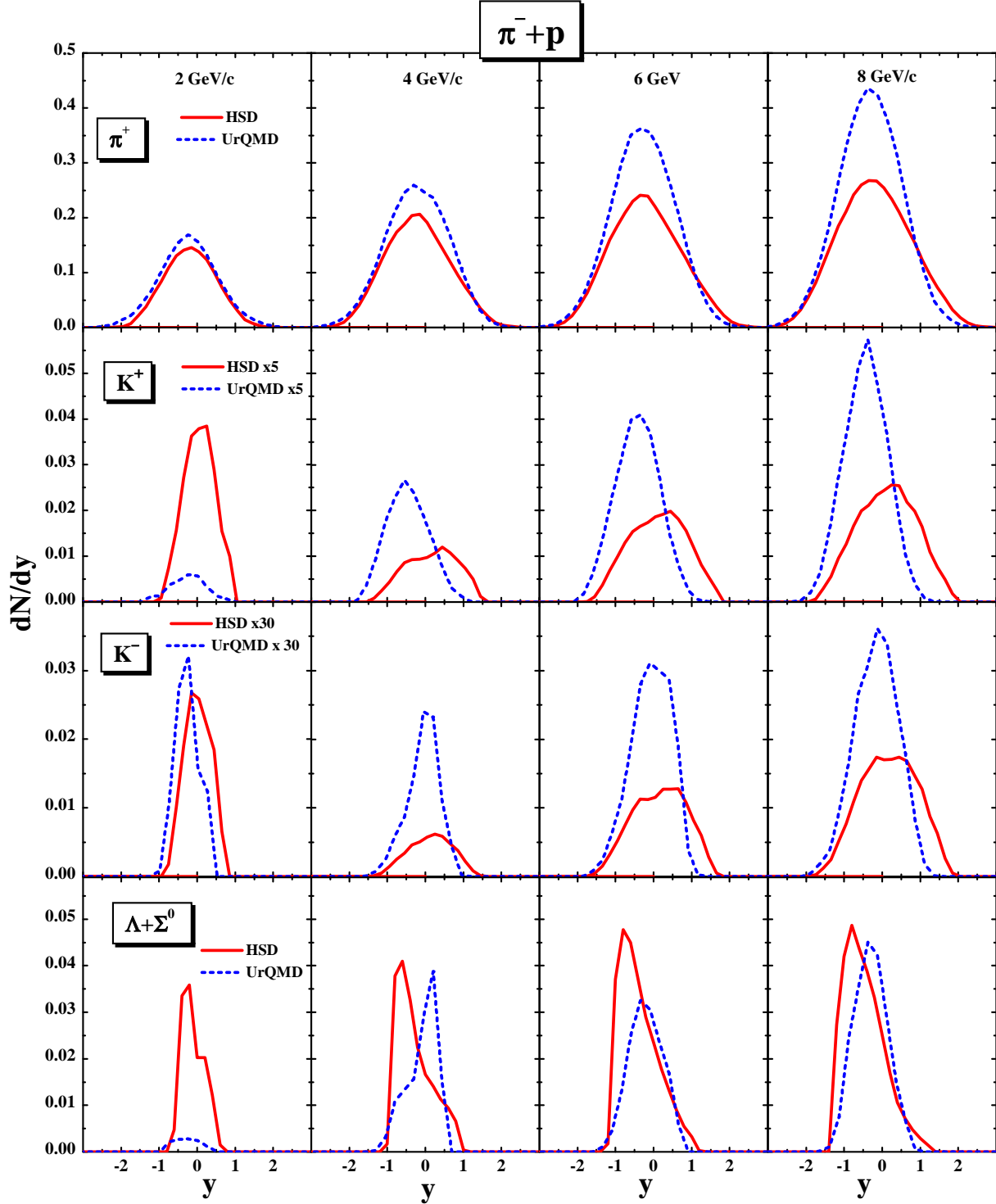
FIG. 14. The rapidity distribution of π^+, K^+, K^- and $\Lambda + \Sigma^0$'s from $\pi^- p$ collisions at 2–8 GeV/c as calculated within HSD (solid lines) and UrQMD (dashed lines). Note, that the K^+ and K^- rapidity distributions from HSD and UrQMD at 2 GeV/c are scaled by factors of 5 and 30, respectively.
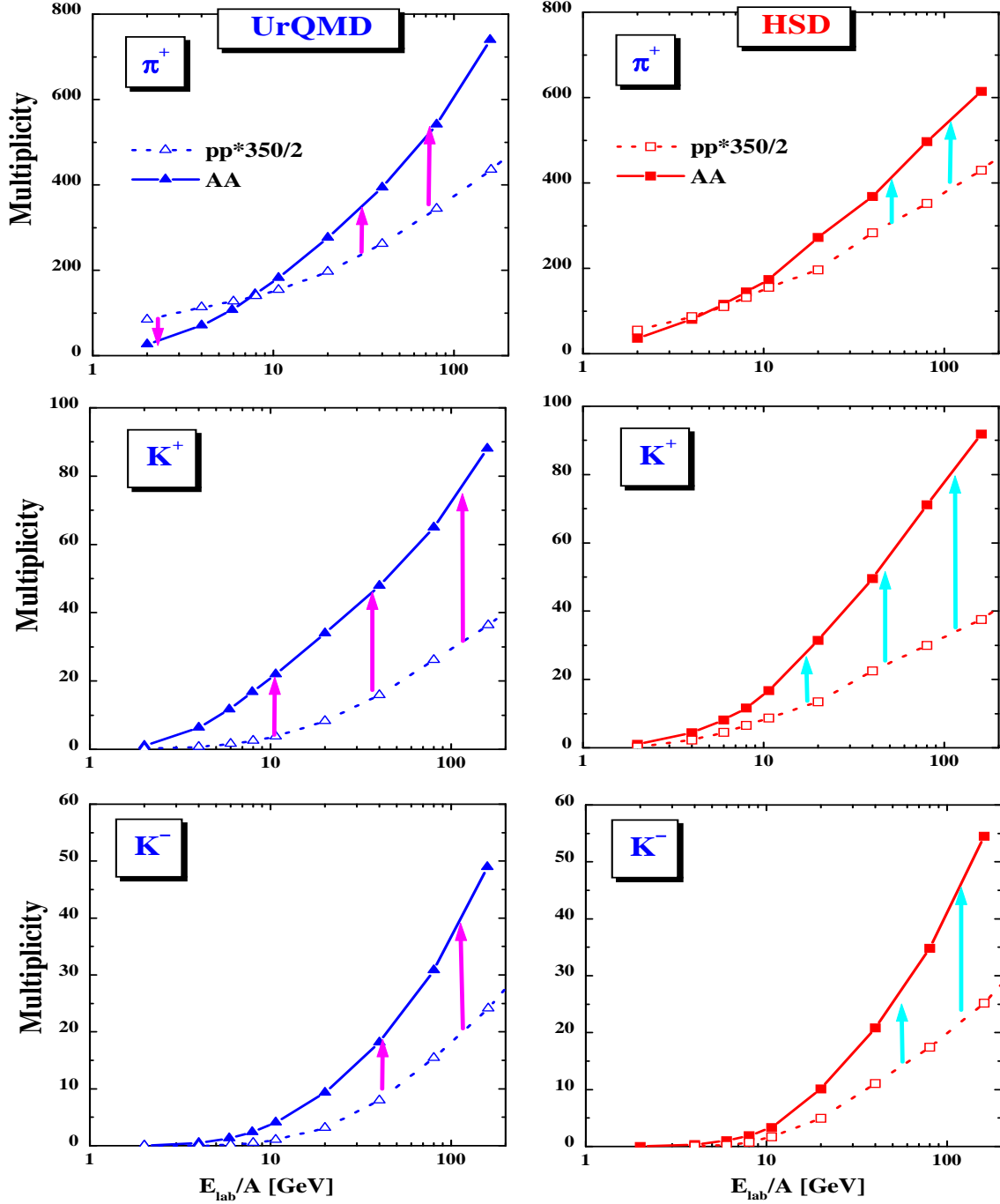
FIG. 15. Total multiplicitis of π^+, K^+ and K^- (i.e. 4π yields) from central $Au + Au$ (at AGS) or $Pb + Pb$ (at SPS) collisions in comparison to the total multiplicities from pp collisions (scaled by a factor 350/2) versus kinetic energy E_{lab}. The solid lines with full triangles and squares show the UrQMD (l.h.s.) and HSD results (r.h.s.) for AA collisions, respectively. The dotted lines with open triangles and squares correspond to the pp multiplicities calculated within UrQMD (l.h.s.) and HSD (r.h.s.).